Mine Impact Burial Model (IMPACT35) Verification and Improvement Using Sediment Bearing Factor Method

Peter C. Chu and Chenwu Fan

Abstract—**Recently, a 3-D model (IMPACT35) *[AU: If it is an acronym, please define]* was developed to predict a falling cylindrical mine's location and orientation in air–water–sediment columns. The model contains the following three components: 1) triple coordinate transform, 2) hydrodynamics of falling rigid object in a single medium (air, water, or sediment) and in multiple media (air–water and water–sediment interfaces), and 3) delta method for sediment resistance with the transient pore pressure. Two mine impact burial experiments were conducted to detect the mine trajectory in water column [Carderock Division, Naval Surface Warfare Center (NSWC), West Bethesda, MD, on September 10–14, 2001], and to measure the mine burial volume in sediment (Baltic Sea in June 2003). The existing IMPACT35 predicts mine's location and orientation in the water column, but not in the sediment column. Since sediment resistance largely affects the mine burial depth and orientation in sediment, a new method (bearing factor) is proposed to compute the sediment resistant force and torque. The improvement of IMPACT35 with the bearing factor method is verified using the data collected from the Baltic Sea mine impact burial experiment. The prediction error satisfies near-Gaussian distribution. The bias of the burial volume (in percent) prediction reduces from 11% using the delta method (old) to 0.1% using the bearing factor method (new). Correspondingly, the root mean square error (rmse) reduces from 26.8% to 15.8%.**

Index Terms—**Author, please supply your own keywords or send a blank e-mail to keywords@ieee.org to receive a list of suggested keywords.**

I. Introduction

THE conclusion of the cold war culminated with the Union of Soviet Socialist Republics (USSR) effectively ceasing to exist under international law on December 31, 1991. This historical event caused the U.S. military and specifically the U.S. Navy and Marine Corp Team to shift tactical emphasis from "blue" water, deep-ocean doctrine to littoral warfare doctrine. This shift predicated military responses dealing with a wide range of worldwide regional crises requiring forward sea basing, and expeditionary force landing support.

Sea mines are big threat in naval operations. Within the past 15 years three U.S. ships, the USS Samuel B. Roberts (FFG-58), Tripoli (LPH-10), and Princeton (CG-59) have fallen victim to mines. Total ship damage was $125 million while the mines cost approximately $30 000 [1]. Mines have evolved over the years from the dumb "horned" contact mines that damaged the Tripoli and Roberts to ones that are relatively sophisticated—nonmagnetic materials, irregular shapes, anechoic coatings, multiple sensors, and ship count routines. Despite their increased sophistication, mines remain inexpensive and are relatively easy to manufacture, keep, and place.

Accurate mine burial predictions are inherently difficult [2], [3] because of unknown conditions in mine deployment and uncertain environments such as waves, currents, and sediment transports [4]. The U.S. Navy developed operational models to forecast ocean environments for mine burial prediction [5], [6]. Recently, statistical methods such as the Monte Carlo [7] and the expert system methods [4] have been developed. These methods have a core-physical model for falling rigid body through air–water–sediment columns. The U.S. Navy has a 2-D model (IMPACT28) to predict cylinder's trajectory and impact burial. The data collected from the mine impact burial experiment in the surf zone near the Naval Postgraduate School, Monterey, CA, shows overprediction of the burial depth (an order of magnitude larger) using IMPACT28 [8].

A 3-D model (IMPACT35) was recently developed at the Naval Postgraduate School to predict cylinder's trajectory and impact burial [9]–[13]. The dynamical system can be simplified using the following three coordinate systems: earth-fixed coordinate (E-coordinate), cylinder's main axis following coordinate (M-coordinate), and hydrodynamic force following coordinate (F-coordinate). The origin of both M- and F-coordinates is at the cylinder's center of mass (COM). The body forces and their moments are easily calculated using the E-coordinate system. The hydrodynamic forces and their moments are easily computed using the F-coordinate. The cylinder's moments of gyration are simply represented using the M-coordinate. When the mine penetrates into an interface between two media (air–water or water–sediment), the cylinder is decomposed into two parts with each one contacting one medium. The body forces (such as the buoyancy force) and surface forces (such as pressure, hydrodynamic force) are computed separately for the two parts. A fully 3-D model is developed for predicting the translation velocity and orientation of a falling cylindrical

Manuscript received March 28, 2005; revised May 19, 2006; accepted August 8, 2006. This work was supported by the U.S. Office of Naval Research Marine Geosciences Program N0001403WR20178 and N0001404WR20067, by the Naval Oceanographic Office, and by the Naval Postgraduate School. **Guest Editor: M. D. Richardson**.

The authors are with the Naval Ocean Analysis and Prediction Laboratory, Department of Oceanography, Naval Postgraduate School, Monterey, CA 93943 USA (e-mail: pcchu@nps.edu).

Color versions of one or more of the figures in this paper are available online at http://ieeexplore.ieee.org.

Digital Object Identifier 10.1109/JOE.2007.890942

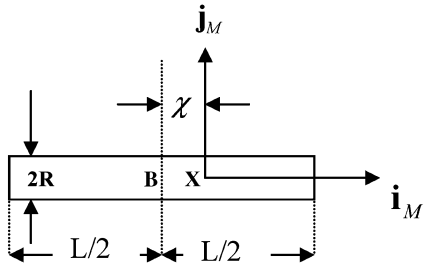

Fig. 1. M-coordinate with the COM as the origin $\mathbf{X}$ and (i_m, j_m) as the two axes. Here, χ is the distance between the COV $(\mathbf{B})$ and COM $(\mathbf{X})$; (L, R) are the cylinder's length and radius.

mine through air, water, and sediment. The value-added capability of the 3-D model (IMPACT35) versus the 2-D model (IMPACT28) is verified using experimental data.

Recently, two mine impact burial experiments were conducted to detect mine trajectory in the water column [Carderock Division, Naval Surface Warfare Center (NSWC), West Bethesda, MD, on September 10–14, 2001] and to measure the mine burial in the sediment (Baltic Sea in June 2003). The collected data are used for model verification. Section II describes basic physics of the recently developed 3-D model (IMPACT35). Section III shows the value-added ***[AU: Change to "added value" throughout?]*** of IMPACT35 in predicting mine movement in water column. However, Section IV shows weakness of the existing IMPACT35 in predicting mine movement in sediment. Section V presents the new bearing factor method to compute the sediment resistant force and torque. Section VI shows the improvement of the bearing factor method in predicting mine burial in sediment. Section VII presents the conclusions.

II. Description of IMPACT35

The 3-D mine impact burial prediction model (IMPACT35) contains the following major components: 1) triple coordinate systems, 2) momentum balance, 3) moment of momentum balance, 4) hydrodynamics, and 5) sediment dynamics. Among them, the hydrodynamics (drag and lift forces and torques) have been described in [9] and [12]–[14], and will not be discussed here.

A. Triple Coordinate Systems

Consider an axially symmetric cylinder with the center of mass (COM) $\mathbf{X}$ and the center of volume (COV) $\mathbf{B}$ on the main axis (Fig. 1). Let (L, R, χ) represent the cylinder's length, radius, and the distance between the two points $(\mathbf{X}, \mathbf{B})$. The positive χ-values refer to nose-down case, i.e., the point $\mathbf{X}$ is lower than the point $\mathbf{B}$. Three coordinate systems are used to model the falling cylinder through the air, water, and sediment phases: earth-fixed coordinate (E-coordinate), main axis following coordinate (M-coordinate), and force following coordinate (F-coordinate) systems. All the systems are 3-D, orthogonal, and right-handed [9].

The E-coordinate system is represented by $F_E(O, \mathbf{i}, \mathbf{j}, \mathbf{k})$ with the origin O, and three axes: x- and y-axes (horizontal)

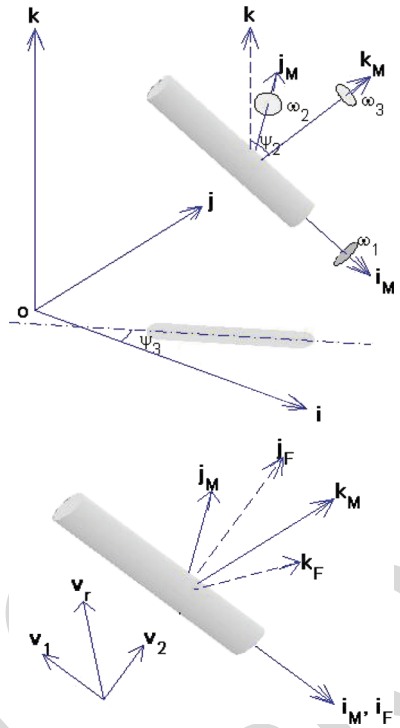

Fig. 2. Three coordinate systems. Here, $(\mathbf{i}, \mathbf{j}, \mathbf{k})$ are the unit vectors of E-coordinate system. Both M- and F-coordinate systems share the same axis, i.e., $\mathbf{i}_M$ and $\mathbf{i}_F$ are the same unit vectors.

with the unit vectors $(\mathbf{i}, \mathbf{j})$ and z-axis (vertical) with the unit vector $\mathbf{k}$ (upward positive). The position of the cylinder is represented by the position of the COM

$$\mathbf{X} = x\mathbf{i} + y\mathbf{j} + z\mathbf{k} \tag{1}$$

which describes translation of the cylinder. The translation velocity is given by

$$\frac{d\mathbf{X}}{dt} = \mathbf{V}, \qquad \mathbf{V} = (u, v, w). \tag{2}$$

Let the orientation of the cylinder's main axis (pointing downward) be given by $\mathbf{i}_M$. The angle between $\mathbf{i}_M$ and $\mathbf{k}$ is denoted by $\psi_2 + \pi/2$. Projection of the vector $\mathbf{i}_M$ onto the (x, y)-plane creates angle (ψ_3) between the projection and the x-axis (Fig. 2). The M-coordinate system is represented by $F_M(\mathbf{X}, \mathbf{i}_M, \mathbf{j}_M, \mathbf{k}_M)$ with the origin $\mathbf{X}$, unit vectors $(\mathbf{i}_M, \mathbf{j}_M, \mathbf{k}_M)$, and coordinates (x_M, y_M, z_M). In the plane consisting of vectors $\mathbf{i}_M$ and $\mathbf{k}$ (passing through the point M), two new unit vectors $(\mathbf{j}_M, \mathbf{k}_M)$ are defined with $\mathbf{j}_M$ perpendicular to the $(\mathbf{i}_M, \mathbf{k})$-plane, and $\mathbf{k}_M$ perpendicular to $\mathbf{i}_M$ in the $(\mathbf{i}_M, \mathbf{k})$-plane. The unit vectors of the M-coordinate system are given by (Fig. 2)

$$\mathbf{j}_M = \mathbf{k}_M \times \mathbf{i}_M, \quad \mathbf{k}_M = \mathbf{i}_M \times \mathbf{j}_M. \tag{3}$$

The M-coordinate system is solely determined by orientation of the cylinder's main axis $\mathbf{i}_M$.

The F-coordinate system is represented by $F_F(\mathbf{X}, \mathbf{i}_F, \mathbf{j}_F, \mathbf{k}_F)$ with the origin $\mathbf{X}$, unit vectors

TABLE I
PHYSICAL PARAMETERS OF THE MODEL MINES IN THE NSWC-CARDEROCK EXPERIMENT (AFTER [20])

Mine	Mass (kg)	ρ (10^3 kg m^{-3})	L (m)	J_1 (kg m^2)	J_2 (J_3) (kg m^2)	χ (m)
1	16.96	1.60	0.505	0.0647	0.356	0
2	22.27	2.10	0.505	0.0806	0.477	0
3	34.93	1.60	1.010	0.1362	2.900	0
4	45.85	2.10	1.010	0.1696	3.820	0
5	45.85	2.10	1.010	0.1693	3.940	0.0045
6	45.85	2.10	1.010	0.1692	4.570	-0.077

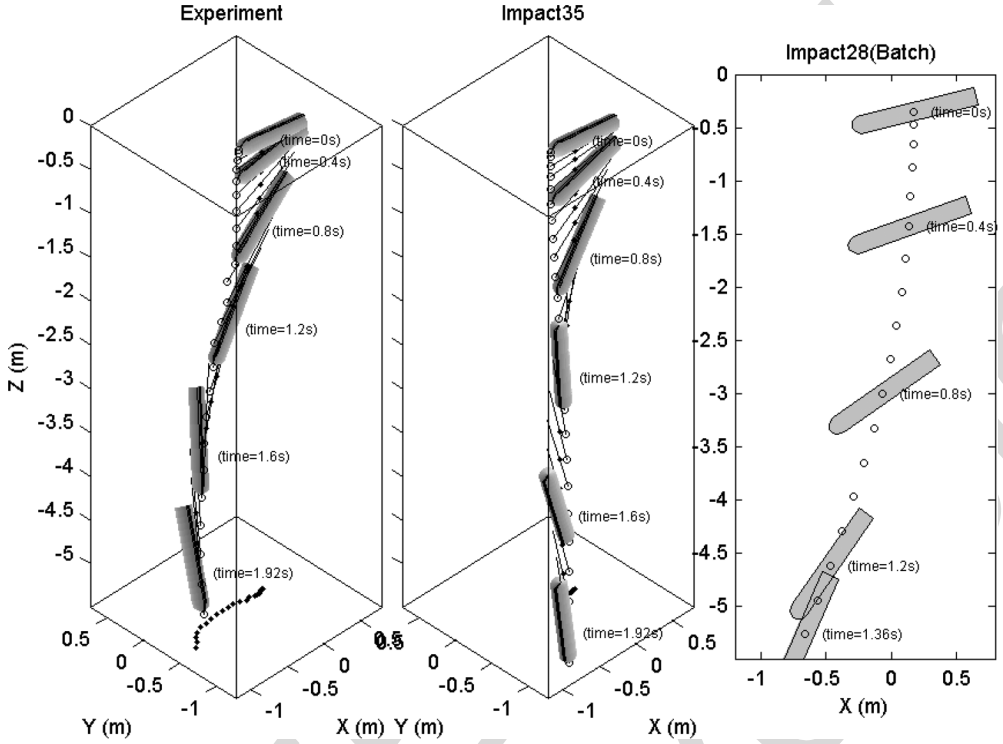

Fig. 3. Movement of mine #6 ($L = 1.01$ m, $\rho = 2.1 \times 10^3$ kg m^{-3}) with $\chi = -0.0077$ m and $\psi_2 = -14.0°$ obtained from (a) NSWC-Carderock experiment, (b) 3-D IMPACT35 model, and (c) 2-D IMPACT28 model. **AU: Please add space between number and unit in Figs. 3, 4, 5.**

$(\mathbf{i}_F, \mathbf{j}_F, \mathbf{k}_F)$, and coordinates (x_F, y_F, z_F). Let $\mathbf{V}_w$ be the fluid velocity. The fluid-to-cylinder velocity is represented by $\mathbf{V}_r = \mathbf{V}_w - \mathbf{V}$, that is decomposed into two parts

$$\mathbf{V}_r = \mathbf{V}_1 + \mathbf{V}_2 \quad \mathbf{V}_1 = V_1 \mathbf{i}_F \quad \mathbf{V}_2 = V_2 \mathbf{j}_F \tag{4}$$

where

$$\mathbf{V}_1 = (\mathbf{V}_r \cdot \mathbf{i}_F)\mathbf{i}_F$$

is the component paralleling to the cylinder's main axis (i.e., along $\mathbf{i}_M$), and

$$\mathbf{V}_2 = \mathbf{V}_r - (\mathbf{V}_r \cdot \mathbf{i}_F)\mathbf{i}_F$$

is the component perpendicular to the cylinder's main-axial direction. The unit vectors for the F-coordinate are defined by (column vectors)

$$\mathbf{i}_F = \mathbf{i}_M = \begin{bmatrix} r_{11} \\ r_{21} \\ r_{31} \end{bmatrix} \quad \mathbf{j}_F = \mathbf{V}_2/|\mathbf{V}_2| \quad \mathbf{k}_F = \mathbf{i}_F \times \mathbf{j}_F. \tag{5}$$

The F-coordinate system is solely determined by orientation of the cylinder's main axis $(\mathbf{i}_M)$ and the water-to-cylinder velocity. Note that the M- and F-coordinate systems have one common unit vector $\mathbf{i}_M$ (orientation of the cylinder). Use of the F-coordinate system simplifies the calculations for the lift and drag forces and torques acting on the cylinder.

B. Momentum Balance

The 3-D translation velocity of the cylinder $(\mathbf{V})$ is governed by the momentum equation in the E-coordinate system [9], [12]–[14]

$$\frac{d}{dt}\begin{bmatrix} u \\ v \\ w \end{bmatrix} = -\begin{bmatrix} 0 \\ 0 \\ g \end{bmatrix} + \frac{\mathbf{F}_{nh} + \mathbf{F}_h}{\rho \Pi} \tag{6}$$

where g is the gravitational acceleration, Π is the cylinder volume, ρ is the rigid body density, $\rho\Pi = m$ is the cylinder mass, $\mathbf{F}_{nh}$ is the nonhydrodynamic force defined later, and $\mathbf{F}_h$ is the hydrodynamic force (i.e., surface force including drag, lift forces). Both $\mathbf{F}_{nh}$ and $\mathbf{F}_h$ are integrated for the cylinder. The drag and lift forces are calculated using the drag and lift

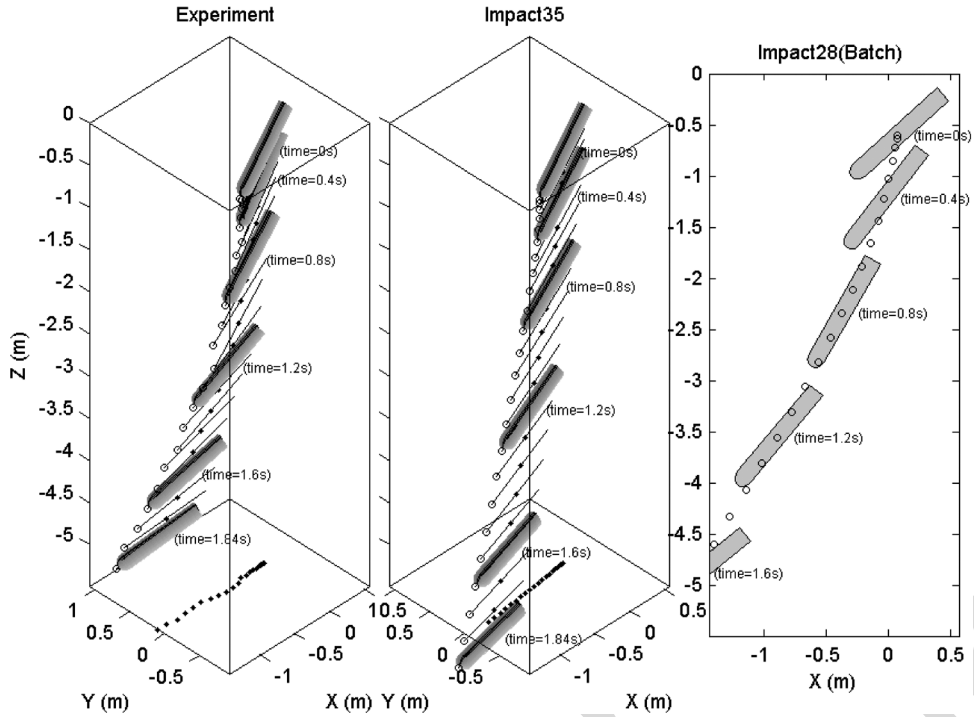

Fig. 4. Movement of mine #5 ($L = 1.01$ m, $\rho = 2.1 \times 10^3$ kg m^{-3}) with $\chi = 0.0045$ m and $\psi_2 = 42.2°$ obtained from (a) NSWC-Carderock experiment, (b) 3-D IMPACT35 model, and (c) 2-D IMPACT28 model.

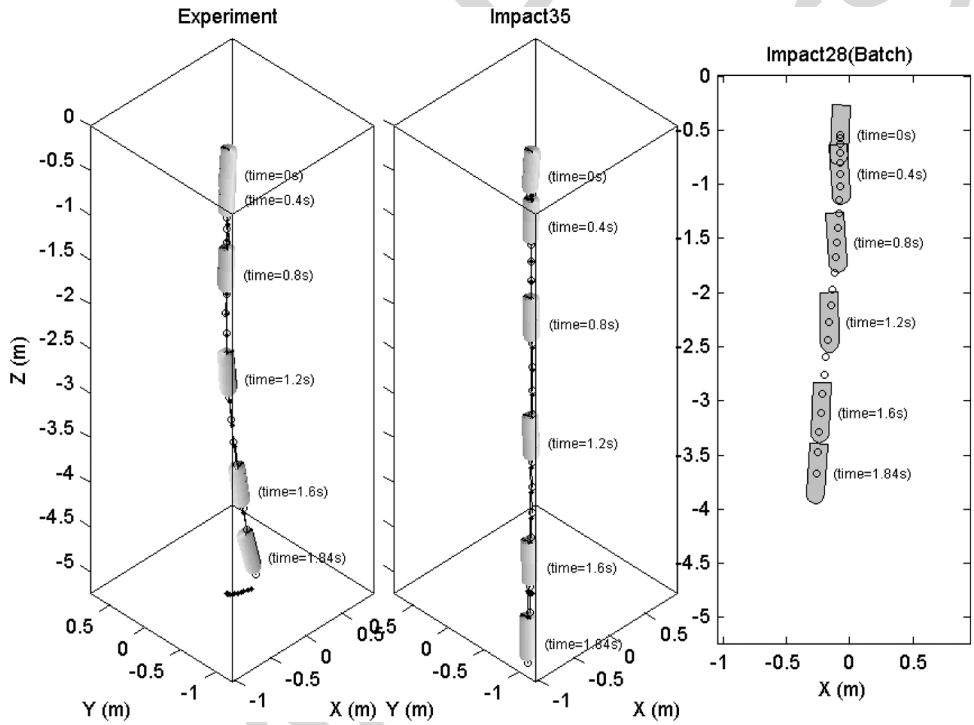

Fig. 5. Movement of mine #2($L = 0.505$ m, $\rho = 2.1 \times 10^3$ kg m^{-3}) with $\chi = 0$ and $\psi_2 = 87.0°$ obtained from (a) NSWC-Carderock experiment, (b) 3-D IMPACT35 model, and (c) 2-D IMPACT28 model.

laws with the given water-to-cylinder velocity $(\mathbf{V}_r)$. In the F-coordinate, $\mathbf{V}_r$ is decomposed into along-cylinder $(\mathbf{V}_1)$ and across-cylinder $(\mathbf{V}_2)$ components. The nonhydrodynamic force $\mathbf{F}_{nh}$ is the buoyancy force $(\mathbf{F}_b)$ for the air and water phases

$$\mathbf{F}_{nh} = \mathbf{F}_b = \mathbf{k}(\rho_a \Pi g, \rho_w \Pi g) \tag{7}$$

where (ρ_a, ρ_w) are the air and water densities and $\mathbf{F}_{nh}$ is the resultant of buoyancy force $(\mathbf{F}_b)$, and shearing resistance force $(\mathbf{F}_s)$ for the sediment phase. ***[AU: Eq. (9) followed (7) in the original. It was changed to (8) and all following eq. numbers were changed accordingly. Please check.]***

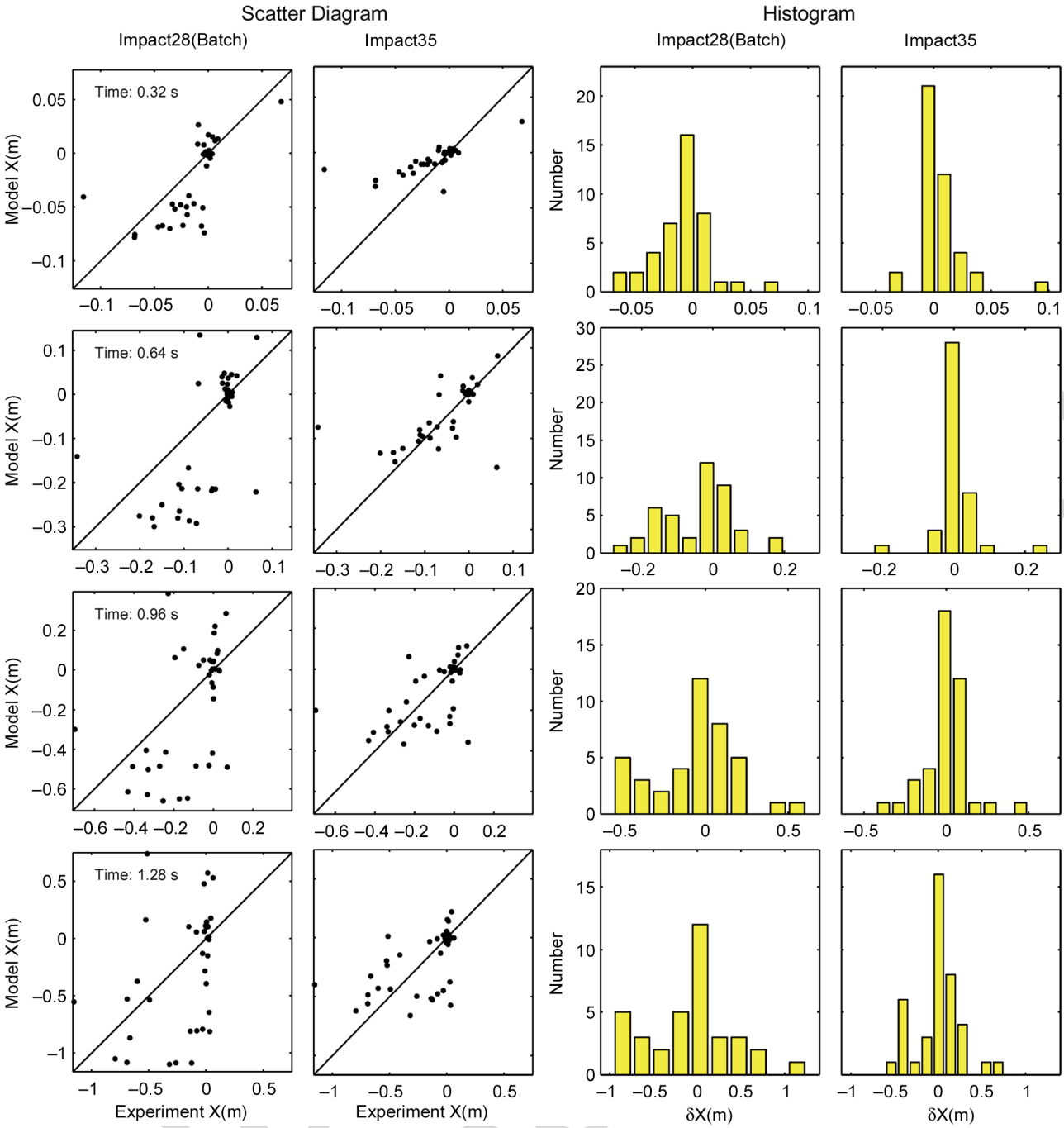

Fig. 6. Model verification from prediction of the COM position x using the NSWC-Carderock experiment data at several time instances: 0.32, 0.64, 0.96, and 1.28 s. Here, the first column is the data-IMPACT28 comparison, the second column is the data-IMPACT35 comparison, the third column shows the histograms of the model error (δx) for IMPACT28, and the fourth column shows the histograms of the model error (δx) for IMPACT35.

C. Moment of Momentum Equation

The moment of momentum equation is written in the M-coordinate system, which rotates with the angular velocity of

$$\mathbf{\Omega} = \omega_2 \mathbf{j}_M + \omega_3 \mathbf{k}_M. \tag{8}$$

Usually, the angular velocity around the mine's main axis $\mathbf{i}_M$ (i.e., self-spinning velocity) is very small $(\omega_1 \simeq 0)$ and neglected. Thus, we have

$$\mathbf{\Omega} = \boldsymbol{\omega}.$$

This leads to zero centripetal and "Coriolis" terms

$$\mathbf{\Omega} \times (\mathbf{\Omega} \times \boldsymbol{\omega}) = 0 \quad -2\mathbf{J} \bullet (\mathbf{\Omega} \times \boldsymbol{\omega}) = 0. \tag{9}$$

The inertial term

$$\frac{d\mathbf{\Omega}}{dt} \times \boldsymbol{\omega} = \mathbf{i}_M \left(\omega_3 \frac{d\omega_2}{dt} - \omega_2 \frac{d\omega_3}{dt} \right) \tag{10}$$

only has the component along the direction of $\mathbf{i}_M$ (mine's main axis). This term may be neglected when the self-spinning

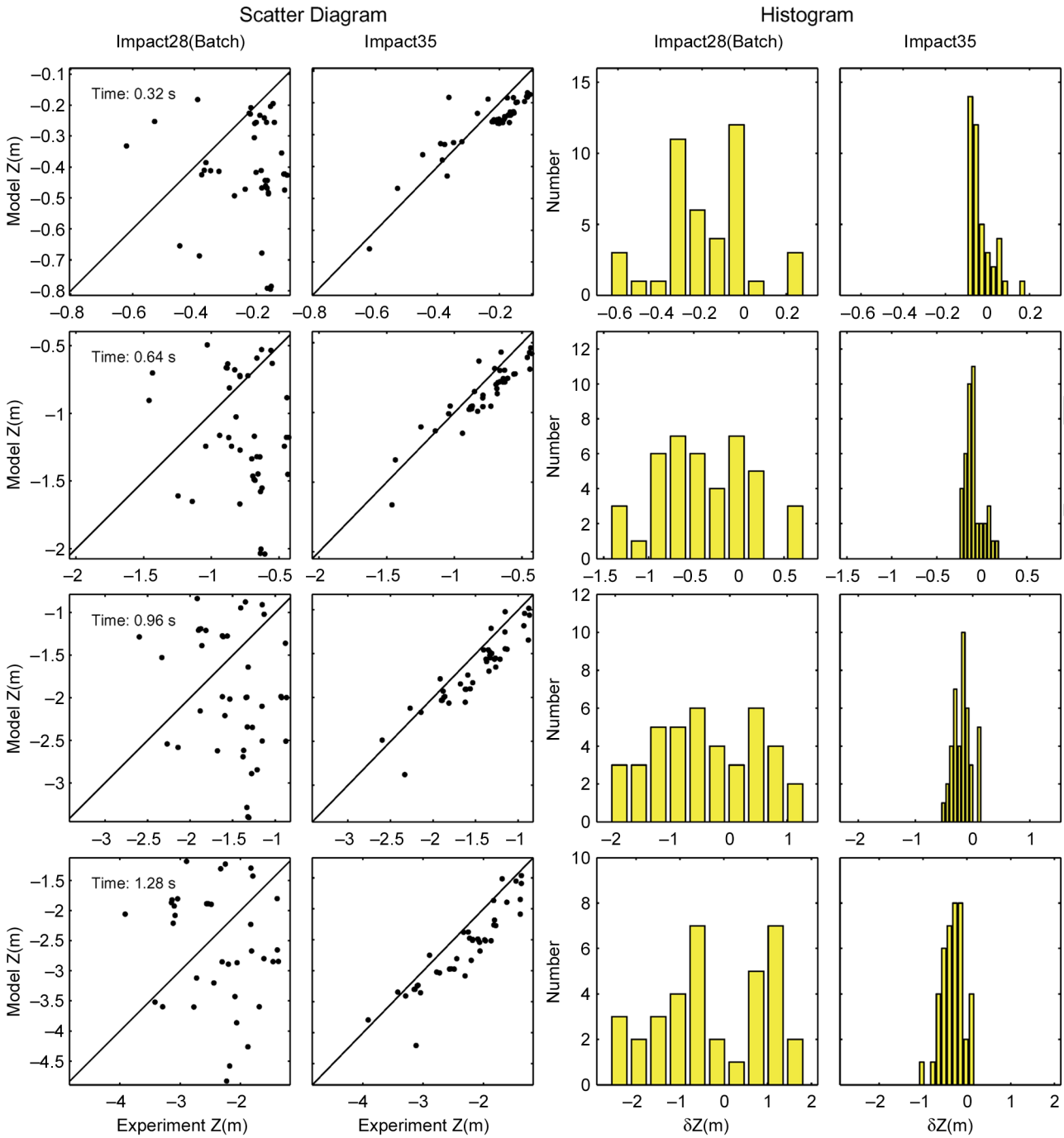

Fig. 7. Model verification from prediction of the COM position z using the NSWC-Carderock experiment data at several time instances: 0.32, 0.64, 0.96, and 1.28 s. Here, the first column is the data-IMPACT28 comparison, the second column is the data-IMPACT35 comparison, the third column shows the histograms of the model error (δx) for IMPACT28, and the fourth column shows the histograms of the model error (δx) for IMPACT35.

velocity is small. The moment of momentum equation in the M-coordinate system can be simplified by

$$\mathbf{J} \bullet \frac{d\boldsymbol{\omega}}{dt} \simeq \mathbf{M}_{nh} + \mathbf{M}_h \tag{11}$$

where $\mathbf{M}_{nh}$ and $\mathbf{M}_h$ are the nonhydrodynamic and hydrodynamic force torques. In the M-coordinate system, the moment of gyration tensor for the axially symmetric cylinder is a diagonal matrix

$$\mathbf{J} = \begin{bmatrix} J_1 & 0 & 0 \\ 0 & J_2 & 0 \\ 0 & 0 & J_3 \end{bmatrix} \tag{12}$$

where J_1, J_2, and J_3 are the moments of inertia. The nonhydrodynamic force usually contains the gravity and buoyancy forces.

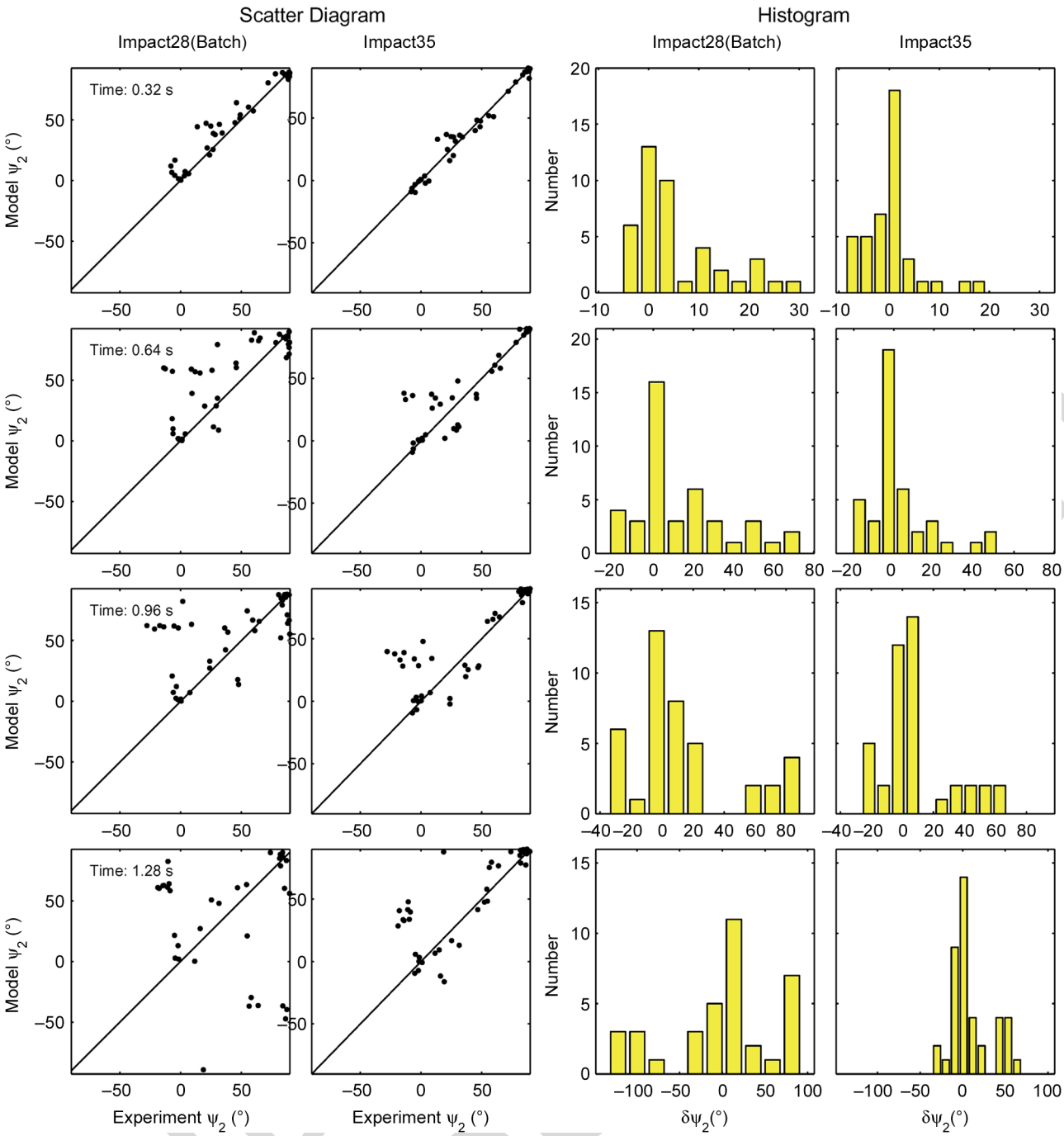

Fig. 8. Model verification from prediction of the orientation ψ_2 using the NSWC-Carderock experiment data at several time instances: 0.32, 0.64, 0.96, and 1.28 s. Here, the first column is the data-IMPACT28 comparison, the second column is the data-IMPACT35 comparison, the third column shows the histograms of the model error $(\delta\psi_2)$ for IMPACT28, and the fourth column shows the histograms of the model error $(\delta\psi_2)$ for IMPACT35.

The gravity force, passing the COM, does not induce the moment. The buoyancy force induces the moment in the $\mathbf{j}_M$ direction if the COM does not coincide with the COV (i.e., $\chi \neq 0$)

$$\mathbf{M}_b = |\mathbf{F}_b|\chi \cos\psi_2 \mathbf{j}_M. \tag{13}$$

D. Sediment Dynamics

In the existing IMPACT35 model, the sediment resistance is calculated using the delta method. This method is on the base on the assumption that the cylinder pushes the sediment and leaves space in the wake as it impacts and penetrates into the sediment. This space is refilled by water and the water cavity is produced. At the instance of the penetration, the total resistant force on the cylinder is represented by [17]–[19]

$$\mathbf{F}^s = \int_{\sigma_{\text{sed}}} \left[\delta\left(\mathbf{f}_b^s + \mathbf{f}_{sh}\right) + \mathbf{f}_b^w + \mathbf{f}_h^w\right] d\sigma + \mathbf{F}_{pw} \tag{14}$$

where $(\mathbf{f}_b^s, \mathbf{f}_{sh})$ and $(\mathbf{f}_b^w, \mathbf{f}_h^w)$ are the sediment buoyancy and shear resistance forces and water buoyancy and hydrodynamic forces (per unit area) at the point $\mathbf{r}$ over the cylinder's surface,

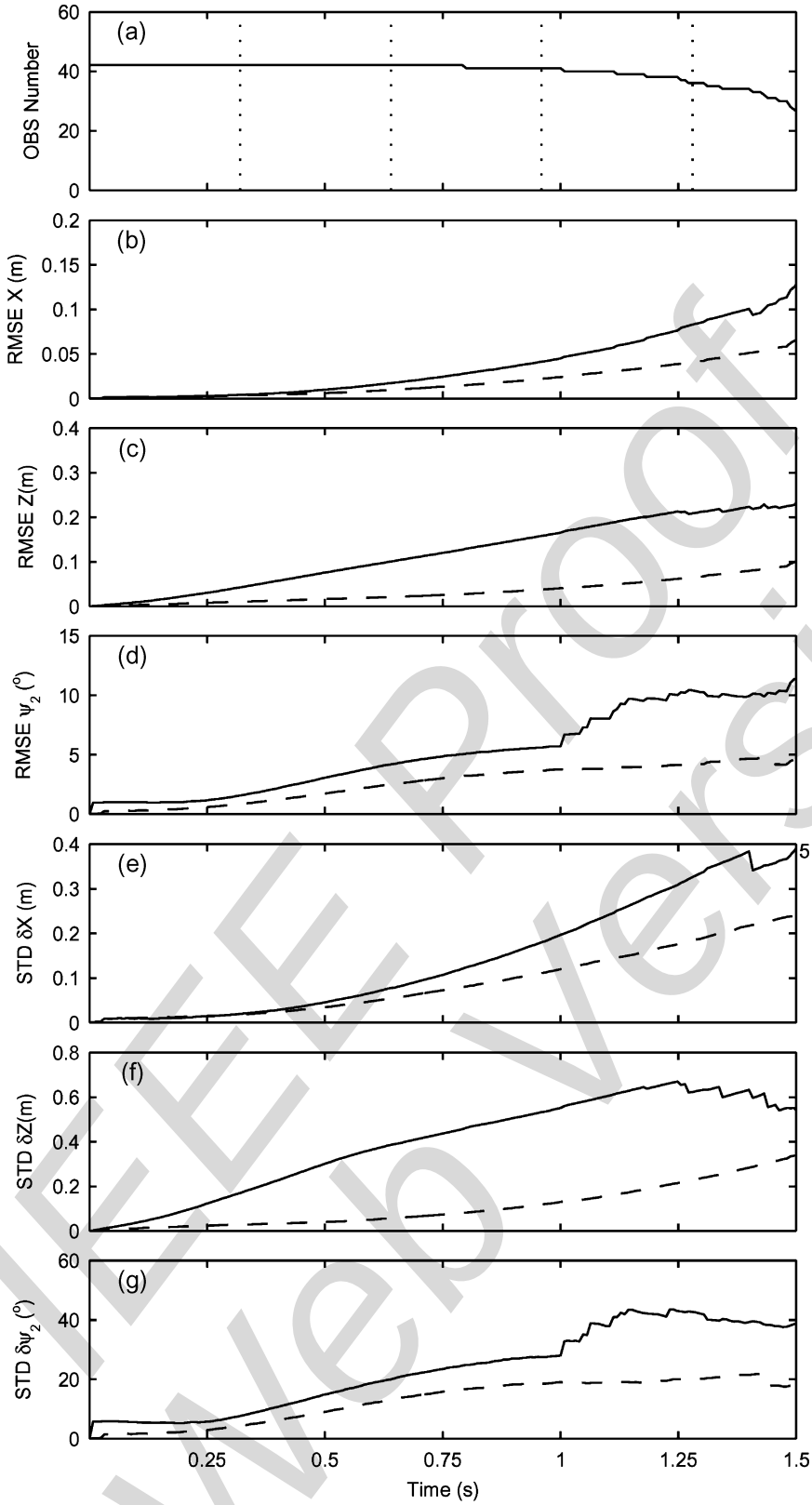

Fig. 9. Temporal evolution of model performance evaluated using the NSWC-Carderock data: (a) observational data number, (b) rmse of x, (c) rmse of z, (d) rmse of ψ_2, (e) STD of δx, (f) STD of δz, and (g) STD of $\delta\psi_2$ with the solid curves for IMPACT35 and dashed curves for IMPACT28 from (b) to (g). **AU: Please change "RMSE" to "rmse" as per IEEE style.**

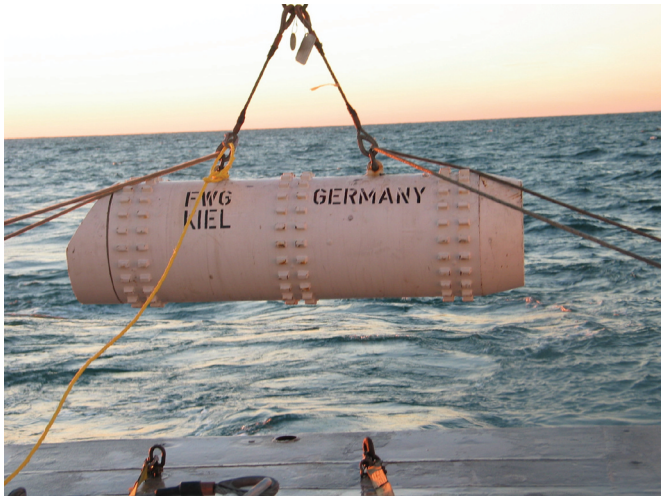

Fig. 10. Optical mine used in the Baltic Sea experiment (after [25]).

TABLE II
PHYSICAL PARAMETERS OF THE FULL-SIZE OPTICAL MINE IN THE BALTIC SEA EXPERIMENT (AFTER [25])

Length (m)	1.466
Diameter (m)	0.470
Taper Diameter (m)	0.395
Taper Length (m)	0.150
Volume (m^3)	0.252
Mass (kg)	550.00
χ (m)	0
J_1 (kg m^2)	14.82
J_2, J_3 (kg m^2)	105.00

TABLE III
PHYSICAL PARAMETERS OF THE ENVIRONMENT IN THE BALTIC SEA EXPERIMENT (AFTER [25])

Air Density (kg m^{-3})	1.22
Water Density (kg m^{-3})	1025.8
Air Kinetic Viscosity (m^2 s^{-1})	1.46×10^{-5}
Water Kinetic Viscosity (m^2 s^{-1})	1.13×10^{-6}

σ_{sed} is the area of the cylinder's surface below the water–sediment interface, $\mathbf{F}_{pw}$ is the pore water pressure force on the whole cylinder, and δ-function is defined by

$$\delta = \begin{cases} 1 & \mathbf{v} \bullet \mathbf{n} \geq 0 \\ 0 & \mathbf{v} \bullet \mathbf{n} \leq 0 \end{cases} \tag{15}$$

which shows that the sediment buoyancy and shear resistance forces act when the cylinder moves towards them. Here, $\mathbf{v}$ is the velocity at point $\mathbf{r}$ (represented in the M-coordinate) on the cylinder surface

$$\mathbf{v} = \mathbf{V} + \boldsymbol{\omega} \times \mathbf{r}. \tag{16}$$

III. VERIFICATION OF IMPACT35 IN THE WATER COLUMN

The NSWC–Carderock experiment was conducted on September 10-14, 2001 in the Explosion Test Pond, which is the only explosive-related test pond in the United States with the capability of providing high-speed underwater photography given its exceptional water clarity. In addition, the facility concrete floor thickness and reinforcement is sufficient to allow impact of 45-kg cylinders without additional floor protection. The pond in plan view is a regular pentagon with each side of 41 m. During the experiment, six model mines (Table I) with mass varying from 16.96 to 45.85 kg were released to the pond with the water depth at 7.92 m [20], [21]. The data set collected from the NSWC-Carderock experiment was used to evaluate value-added of IMPACT35 versus IMPACT28 (2-D model).

A. Near Horizontal Release

Model mine #6 was released to the water with $\psi_2 = -14°$ (near horizontal, see Fig. 2). The physical parameters of this mine are given by

$$\begin{aligned} &L{=}1.01\text{ m} \quad \rho{=}2.10\times10^3\text{ kg m}^{-3} \quad \chi{=}-0.077\text{ m} \\ &m{=}45.85\text{ kg} \quad J_1{=}0.1692\text{ kg m}^2 \quad J_2{=}J_3{=}4.570\text{ kg m}^2. \end{aligned} \tag{17}$$

The initial conditions are given by

$$\begin{aligned} &x_0 = y_0 = z_0 = 0 \quad u_0 = v_0 = w_0 = 0 \\ &r\psi_{10} = 0 \quad \psi_{20} = -14° \quad \psi_{30} = 0 \quad \omega_{10} = \omega_{20} = \omega_{30} = 0. \end{aligned} \tag{18}$$

Substitution of the model parameters (17) and the initial conditions (18) into IMPACT28 and IMPACT35 leads to the prediction of the mine's translation and orientation that are compared with the data collected during the experiment at each time step (Fig. 3). The new 3-D model (IMPACT35) simulated trajectory agrees well with the observed trajectory. Both show the same pattern and the same travel time (1.92 s) for the cylinder passing through the water column. However, the 3-D model (IMPACT35) is better than the 2-D model (IMPACT28) in predicting the mine's movement in the water column.

B. Near 45° Release

Model mine #6 was released to the water with $\psi_2 = 42.2°$. The initial conditions are given by

$$\begin{aligned} &x_0{=}y_0{=}z_0{=}0 \quad u_0{=}v_0{=}w_0{=}0 \\ &\psi_{10}{=}0 \quad \psi_{20}{=}42.2° \quad \psi_{30}{=}0 \quad \omega_{10}{=}\omega_{20}{=}\omega_{30}{=}0. \end{aligned} \tag{19}$$

Substitution of the model parameters (17) and the initial conditions (19) into IMPACT28 and IMPACT35 leads to the prediction of the mine's translation and orientation that are compared with the data collected during the experiment at time steps (Fig. 4). Both 3-D model (IMPACT35) and 2-D model (IMPACT28) simulated trajectories and travel times agree well with the observed trajectory.

C. Near Vertical Release

Model mine #2 was released to the water with $\psi_2 = 87°$. The physical parameters of this mine are given by

$$\begin{aligned} &L = 0.505\text{ m} \quad \rho = 2.10\times10^3\text{ kg m}^{-3} \quad \chi = 0 \\ &m = 22.27\text{ kg} \quad J_1 = 0.0806\text{ kg m}^2 \\ &J_2 = J_3 = 0.477\text{ kg m}^2. \end{aligned} \tag{20}$$

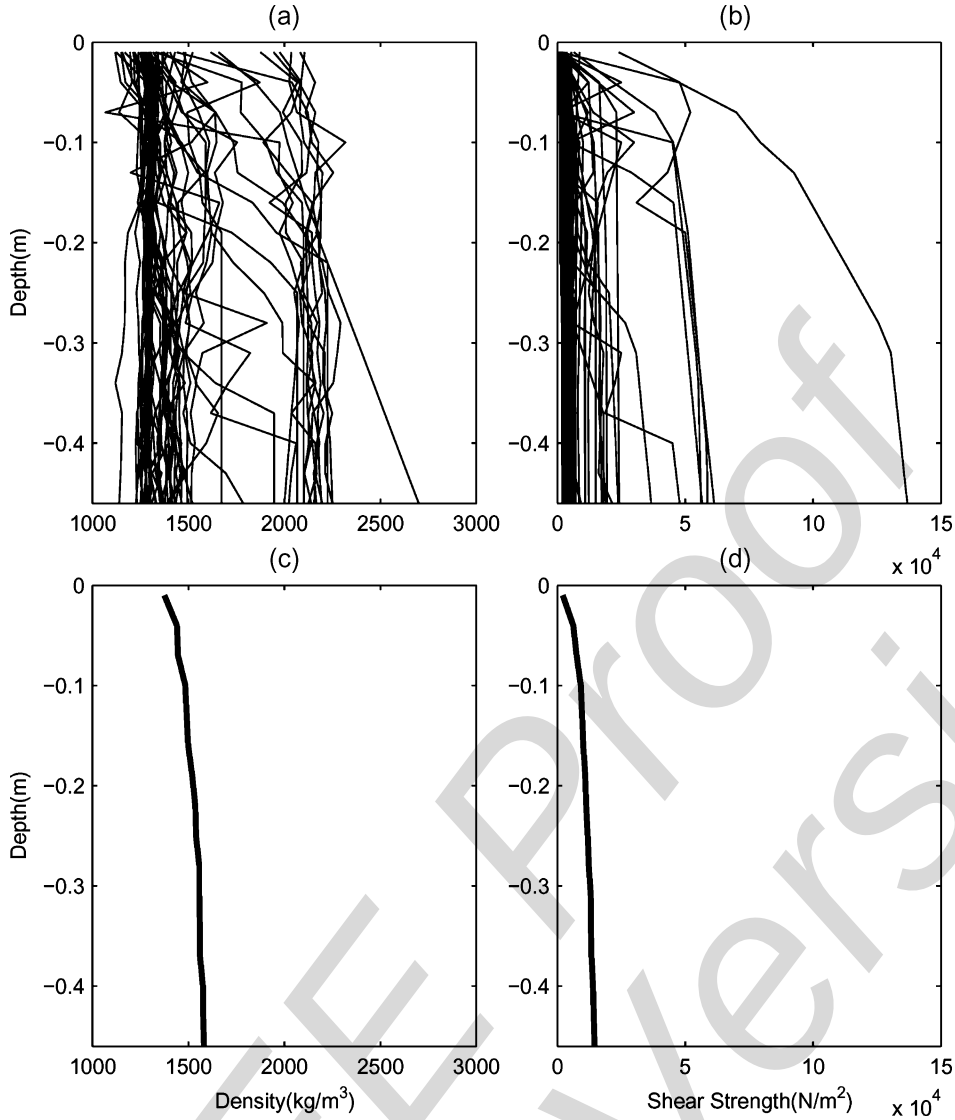

Fig. 11. Sediment density $\rho_s(z)$ and static shear strength $S(z)$ profiles in the Baltic Sea from the cores collected at 59 mine impact sites during the mine-drop experiment in June 2003: (a) individual density profiles, (b) individual static shear strength profiles, (c) mean density profile, and (d) mean static shear strength profile (after [25]). **AU: Should "kg/m^3" be "kg m^3" and "N/m^2" " N m^2? If yes, please provide new figure.**

The initial conditions are given by

$$x_0 = y_0 = z_0 = 0 \quad u_0 = v_0 = w_0 = 0$$
$$\psi_{10} = 0 \quad \psi_{20} = 87^\circ \quad \psi_{30} = 0 \quad \omega_{10} = \omega_{20} = \omega_{30} = 0. \quad (21)$$

The predicted cylinder's translation and orientation are compared with the data collected at time steps (Fig. 5). The 3-D model (IMPACT35) simulated trajectory agrees well with the observed trajectory. Both show the same straight pattern and the same travel time (1.84 s) for the cylinder passing through the water column.

D. Statistical Error Analysis

Figs. 6–8 show scatter diagrams and histograms for predicting mine's location and orientation $[x(t), z(t), \psi_2(t)]$. In the scatter diagrams, the points cluster around the diagonal line of $\varsigma_m = \varsigma_o$ using IMPACT35 (second column), and the points are spreading out of the diagonal line using IMPACT28 (first column), which confirms that IMPACT35 predicts COM position more accurately than IMPACT28. Histograms of model errors for COM position have Gaussian-type distribution with near-zero mean and small standard deviation (STD) using IMPACT35 (fourth column), and non-Gaussian-type distributions with large STD using IMPACT28 (third column).

The total number of observational points at each time instance $N(t)$ is around 41 as t <1.2 s and reduces quickly with time as t >1.2 s Fig. 9(a), which indicates that the model verification is reliable for t <1.2 s. The value-added of IMPACT35 is easily seen from Fig. 9. For example, the root mean square error (rmse) of COM prediction is much smaller when using IMPACT35 than IMPACT28 [Fig. 9(b) and (c)]. The STDs of the model errors for the COM prediction are also much lower when using IMPACT35 than IMPACT28 [Fig. 9(e) and (f)]. The rmse of orientation prediction is smaller when using IMPACT35 than IMPACT28 for t <1 s. When t >1 s, the rmse

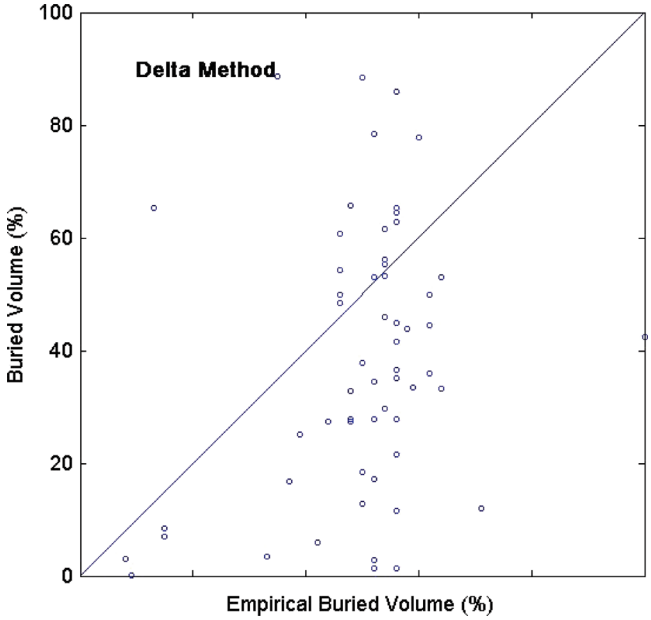

Fig. 12. Scatter diagrams of buried volume prediction against the Baltic Sea experimental data. Here, IMPACT35 uses the delta method for sediment resistance.

of ψ_2 is around half when using IMPACT35 than when using IMPACT28 [Figs. (9d) and (g)].

IV. Verification of IMPACT35 in Sediment

The Baltic Sea experiment was conducted in June 2003 by the German Federal Armed Forces Underwater Acoustic and Marine Geophysics Research Institute (FWG, Kiel, Germany) [22] with the full-size optical mine (Fig. 10) which is allowed to free fall from the wench. Table II shows the physical parameters of the optical mine. Table III lists the physical environments in the Baltic Sea. The full-size optical mine was released 59 times. The water depths of the drop sites were between 25.0 and 26.5 m (Fig. 11). The volume of mine burial percentage was measured. The readers are referred to [7] for detailed information.

After running IMPACT35 with the delta method for the sediment resistance (14) for each gravity core regime $[\rho_s(z), S(z)]$, the predicted and observed burial volumes (in percent) were compared (Fig. 12). The bias (mean predicted minus observed values) and rmse of burial volume are 11% and 26.8%. The correlation coefficient between predicted and observed burial volumes is 0.374%.

The histograms of the burial volume (in percent) are very different between the Baltic Sea experiment and the model prediction of IMPACT35 using the delta method [Fig. 13(a) and (b)]. In the experiment, the probability density function (pdf) has a peak at burial volume of 50% with a frequency of 26. However, the model predicted pdf has a peak at 30% with a frequency of 11.

V. Bearing Factor Method

New (bearing factor) method is presented for calculating the sediment resistant force and torque.

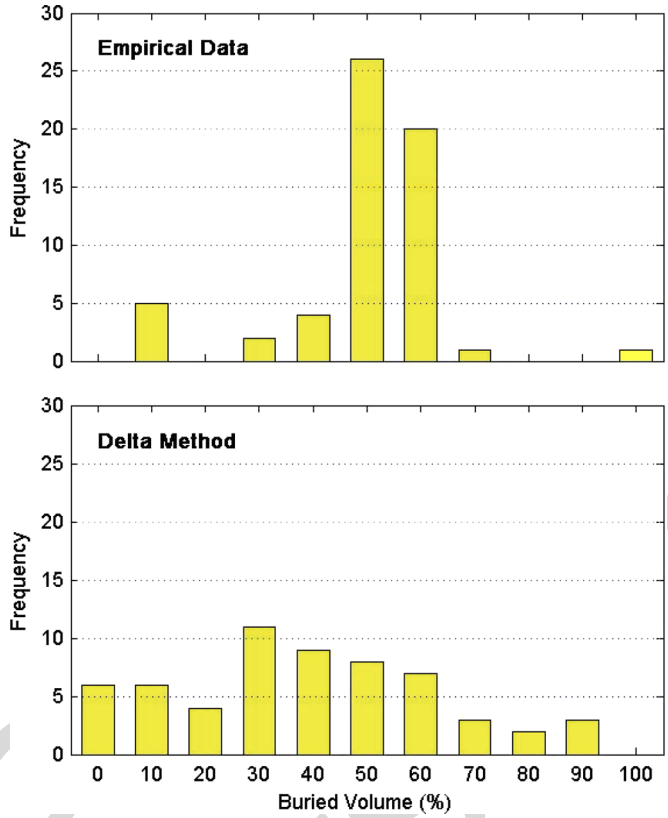

Fig. 13. Histograms of buried volume (in percent) from (a) Baltic Sea experiment and (b) prediction using IMPACT35 with the delta method.

A. Sediment Resistance

When the mine impacts and penetrates into the sediment, it creates a large transient pore pressure in the sediment that causes ruptures in the sediment and influences the resistance force on the cylinder [23], [24]. The resistance of the sediment to mine's penetration is assumed to have the following three components: buoyancy force $\mathbf{F}_b^s$, hydrodynamic (drag and lift) force $\mathbf{F}_h^s$ (similar to air and water), and shear resistance force $\mathbf{F}_r^S$ (resistance to the rupture)

$$\mathbf{F}^s = \mathbf{F}_b^s + \mathbf{F}_h^s + \mathbf{F}_r^s. \tag{22}$$

The sediment buoyancy force per unit area is defined by

$$\mathbf{F}_b^s = -\mathbf{n} \int_z^{z_{ws}} \rho_s(z') g dz' \tag{23}$$

where $\rho_s(z)$ is the sediment wet density (usually obtained from the sediment data), $\mathbf{n}$ is unit vector normal to the mine surface (outward positive), and z_{ws} represents the vertical coordinate of the water–sediment interface.

The shear resistance force $(\mathbf{F}_r^S)$ is in the opposite direction of $\mathbf{v}$ and acts on the mine. Its magnitude is proportional to the product of the sediment shear strength (S) and the rupture area (A, projection of sediment-contacting area perpendicular to the velocity $\mathbf{V}$) with a nonnegative bearing factor N [16]

$$\mathbf{F}_r^s = -\boldsymbol{\tau} N(p, v) S A, \qquad N \geq 0. \tag{24}$$

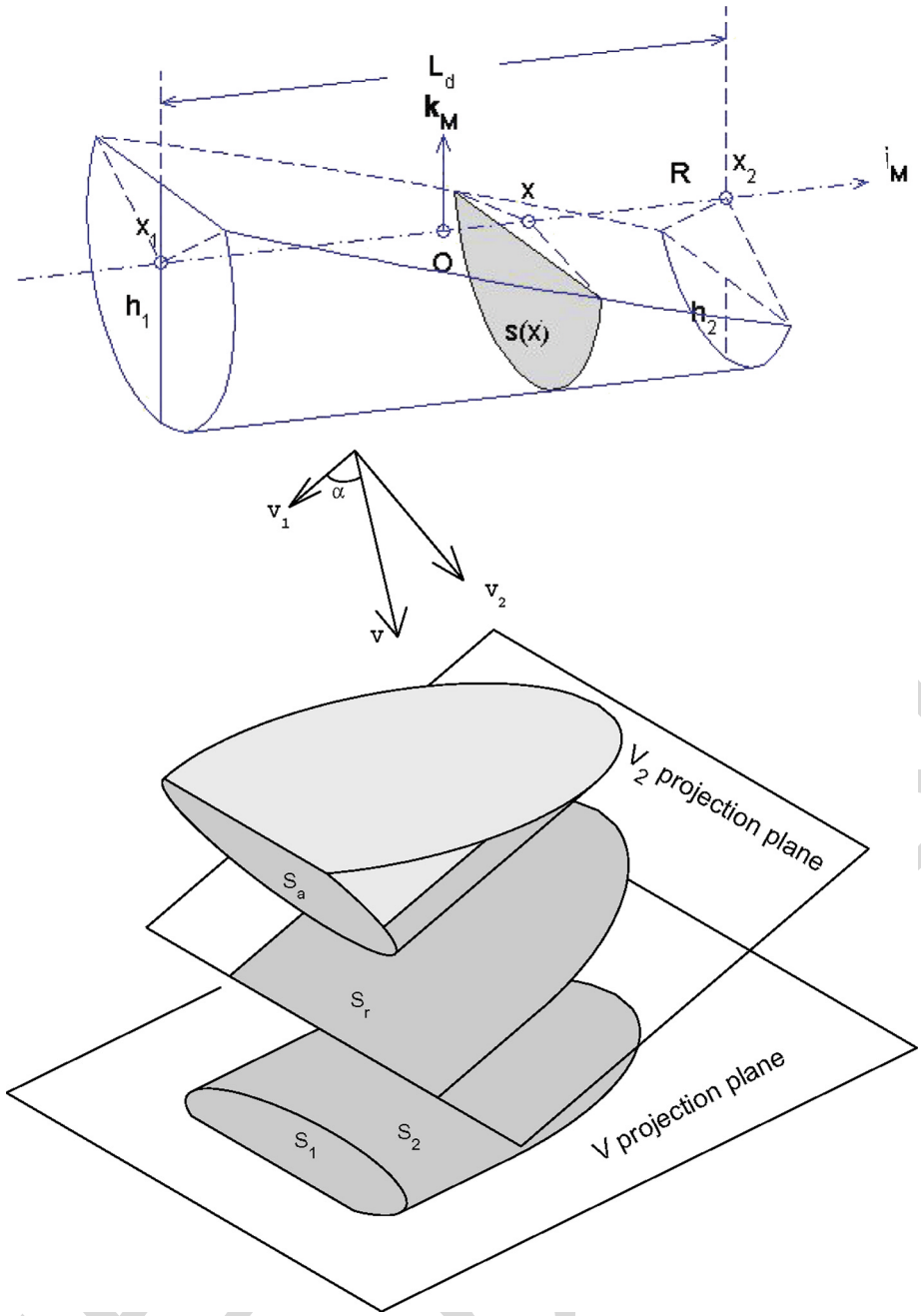

Fig. 14. Calculation of immersed area.

The sediment resistance torque includes the hydrodynamic and shearing resistance torques

$$\mathbf{M}^s = \mathbf{r} \times (\mathbf{F}_r^s + \mathbf{F}_h^s) = -[N(p,v)SA]\,\mathbf{r} \times \boldsymbol{\tau} + \mathbf{r} \times \mathbf{F}_h^s. \quad (25)$$

Here, p is the nondimensional penetration depth scaled by the diameter of the cylinder $(2R)$. The sediment density in (23) and shear strength (S) in (24) and (25) are measured.

The bearing factor increases with p and decreases with the decreasing speed

$$N(p,v) = [\mu_1 p^{\mu_2}] \left[1 + \lambda \log\left(\frac{v}{v_{\text{cri}}}\right)\right] \quad (26)$$

where λ is the v-effect parameter, (μ_1, μ_2) are the p-effect parameters [16], and v_{cri} is the critical speed. The bearing factor N is amplified $[1 + \lambda \log(v/v_{\text{cri}}) > 1]$ for $v > v_{\text{cri}}$, independent of v for $v = v_{\text{cri}}$, and is reduced $[1 + \lambda \log(v/v_{\text{cri}}) < 1]$ for $v < v_{\text{cri}}$. During the penetration, v decreases since the buoyancy, hydrodynamic, and shear resistance forces oppose the penetration. Decrease of v reduces bearing factor N. The two p-effect parameters are given by [16]

$$\mu_1 = 9.3 \quad \mu_2 = 0.7.$$

Note that the nondimensional (26) and the two p-effect parameters are derived from a small probe under axial impact condi-

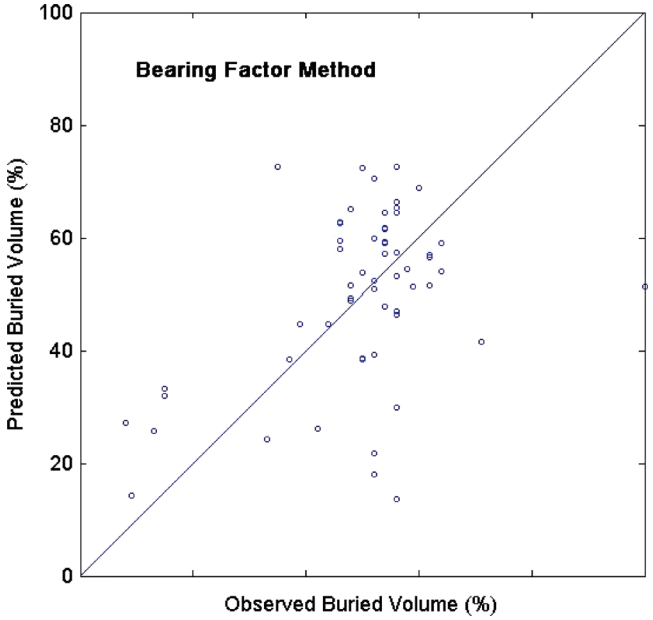

Fig. 15. Scatter diagrams of buried volume prediction against the Baltic Sea Experiment data. Here, IMPACT35 uses the bearing factor method for sediment resistance.

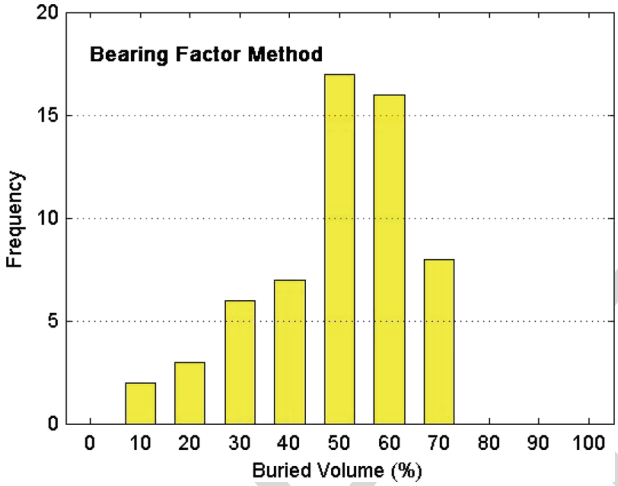

Fig. 16. Histogram of buried volume (in percent) prediction using IMPACT35 with the delta method.

tion. Validity of the bearing factor method to mine impact burial needs thorough evaluation.

Since N cannot be negative, when v decreases to a critical

$$v = v_{\text{cri}} e^{-\frac{1}{\lambda}} \tag{27}$$

the bearing factor $N(p, v)$ and in turn the shearing resistance force become zero. The mine ceases the penetration in sediment. Note that λ and v_{cri} are the two tuning parameters of the numerical model. In this paper, we use

$$\lambda = 0.2 \quad v_{\text{cri}} = 0.0015 \text{ m s}^{-1}. \tag{28}$$

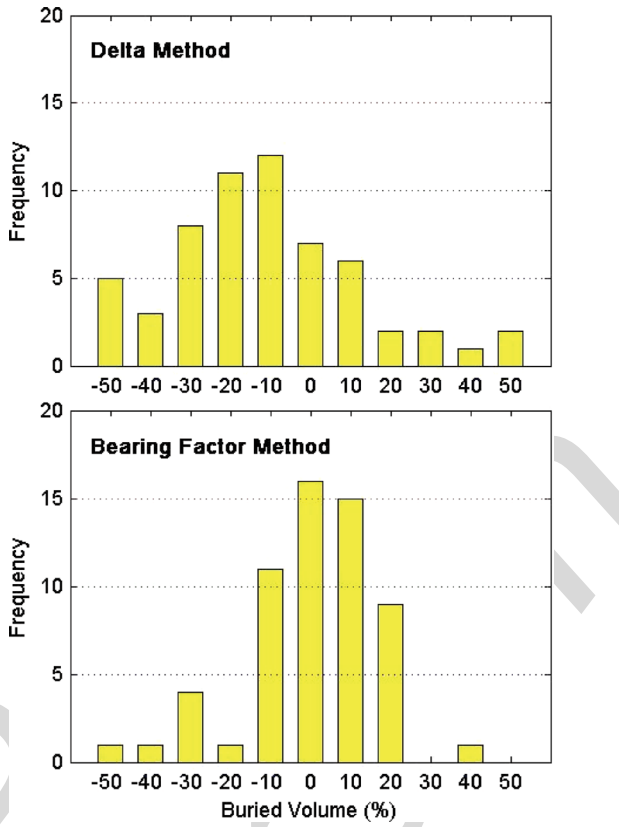

Fig. 17. Histograms of the buried volume prediction error of IMPACT35 using (a) the delta method, and (b) the bearing factor method.

B. Rupture Area

Usually, after passing through the water column, the cylinder's velocity reduces. The rupture area can be represented approximately by the contact surface area. Let (A_f, A_t) be the sediment-contacting areas on the circular bottom (fan shape) and side (curved trapezoid). The rupture area A is the summation of the projections of (A_f, A_t) on the plane perpendicular to the mine's velocity $\mathbf{V}$

$$A = A_1 + A_2 \quad A_1 = A_f \cos\alpha \quad A_2 = A_t \sin\alpha \tag{29}$$

where α is the angle between $\mathbf{V}$ and the mine's axis. Let R be the radius of the cylinder, h be the depth of A_f, and (h_1, h_2) be the depths of the trapezoid A_t immersed in the sediment (Fig. 14). Let the length of the trapezoid be L_t. A_f is computed simply by

$$A_f = \frac{\theta}{2} R^2 - (R-h)\sqrt{R^2-(R-h)^2}, \qquad \theta = \cos^{-1}\left(\frac{R-h}{R}\right). \tag{30}$$

A_t is computed by

$$A_t = \begin{cases} 2L_t R, & \text{for } h_1 > h_2 \geq R \\ \frac{L_t}{(h_1 - h_2)}\left[R^2(\theta_1 - \theta_2)\right. & \\ \quad \left. -(R-h_1)b_1 + (R-h_2)b_2\right], & \text{for } h_2 < h_1 \leq R \\ 2L_{t1}R + \frac{L_{t2}}{(R-h_2)} & \\ \quad \times \left[R^2\left(\frac{\pi}{2} - \theta_2\right) + (R-h_2)b_2\right], & \text{for } h_1 > R > h_2 \end{cases} \tag{31}$$

where (L_{t1}, L_{t2}) are the lengths of subcylinders with $(h > R, h < R)$ and b_1 and b_2 are computed by

$$b_1 = \sqrt{R^2 - (R-h_1)^2} \quad b_2 = \sqrt{R^2 - (R-h_2)^2}. \tag{32}$$

VI. Model Improvement Using the Bearing Factor Method

Model improvement is evaluated using the Baltic Sea experiment data. Similar to the process described in Section V, the modeled (with the bearing factor method) and observed burial volumes (in percent) were compared (Fig. 15). As evident, the sediment resistance using the bearing factor method improves the prediction capability of IMPACT35. The bias (mean predicted minus observed values) and rmse of the burial volume reduce to 0.1% and 15.8%. The correlation coefficient between observed and predicted burial volumes increases to 0.435 (using the bearing factor method) from 0.374 (using the delta method).

The histogram of the predicted burial volume (in percent) using the bearing factor method (Fig. 16) is closer to that of the Baltic Sea experiment [Fig. 13(a)] than the histogram of the predicted burial volume (in percent) using the delta method Fig. 13(b). In the experiment, the histogram has a peak at burial volume of 50% with a frequency of 26. In the prediction, the histogram has a peak at 30% with a frequency of 11 using the delta method Fig. 13(b). However, the histogram has a peak at 50% with a frequency of 17% (Fig. 16).

The histogram of the model error is more symmetric around the zero error using the bearing factor method than using the delta method. For example, the histogram has a peak at zero error with frequency of 16 using the bearing factor method [Fig. 17(b)], and a peak at -10% error with the frequency of 12 using the delta method [Fig. 17(a)]. The burial volume prediction is unbiased using the bearing factor method, and negatively biased using the delta method.

VII. Summary

The following points summarize this paper.

1) The 3-D mine impact burial prediction model (IMPACT35) was recently developed to predict the translation and orientation of falling cylindrical mine through air, water, and sediment. It contains the following three components: triple coordinate transform, cylinder decomposition, and hydrodynamics of falling rigid object in a single medium (air, water, or sediment) and in multiple media (air–water and water–sediment interfaces).
2) Data collected from two mine impact burial experiments were used to verify the existing IMPACT35. The predicted mine track and orientation in the water column agree quite well with the NSWC-Caderock data. The rmse of mine's position and orientation is much smaller using IMPACT35 than using IMPACT28. However, the predicted mine burial volume in the sediment was not as good as the mine trajectory in the water column.
3) Calculation of the sediment resistant force and torque is updated from the delta method (old) to the bearing factor method (new). With the bearing factor method, the prediction capability of IMPACT35 has been greatly improved. The prediction error satisfies near-Gaussian distribution. The bias of the burial volume (in percent) prediction reduces from 11% using the delta method (old) to 0.1% using the bearing factor method. Correspondingly, the rmse reduces from 26.8% to 15.8%.
4) IMPACT35 developed in this paper is only for cylindrical mines only. It is necessary to extend the modeling effort to more realistic mine shapes such as Rockan and Manta for operational use.

Acknowledgment

The authors would like to thank Dr. P. Valent and Dr. A. Abelev at the NRL for providing the NSWC-Carderock experiment data, Dr. T. Weaver at the FWG for providing the Baltic Sea experiment data, and the two anonymous reviewers and the editor Dr. M. D. Richardson for comments that improved the manuscript greatly.

References

[1] J. M. Boorda, *Mine Countermeasures—An Integral Part of Our Strategy and Our Forces*. Washington, DC: Federation of American Scientists, 1999 [Online]. Available: http://www.fas.org/man/dod-101/sys/ship/weaps/docs/cnopaper.htm

[2] ***[Page range to come!]*** S. A. Jenkins, D. L. Inman, M. D. Richardson, T. F. Wever, and J. Wasyl, "Scour and burial mechanisms of objects in the nearshore," *IEEE J. Ocean. Eng.*, vol. 32, no. 1, pp. XXX–XXX, Jan. 2007.

[3] ***[Page range to come!]*** P. C. Chu, "Mine impact burial prediction from one to three dimensions," *IEEE J. Ocean. Eng.*, vol. 32, no. 1, pp. XXX–XXX, Jan. 2007.

[4] ***[Page range to come!]*** S. E. Rennie, A. Brandt, and N. Plant, "A probabilistic expert system approach for sea mine burial prediction," *IEEE J. Ocean. Eng.*, vol. 32, no. 1, pp. XXX–XXX, Jan. 2007.

[5] S. Haeger, "Operational ocean modeling support for mine warfare in operation Iraqi freedom," in *Proc. 6th Int. Symp. Technol. Mine Problem*, Monterey, CA, May 10–13, 2004, DVD-ROM.

[6] ***[AU: Please provide page range]*** P. Fleischer, "Mine burial prediction NAVOCEANO perspective," in *Proc. 5th Annu.ONR Workshop Mine Burial Prediction*, Kona, HI, Jan. 31–Feb. 2 2005.

[7] ***[Page range to come!]*** P. A. Elmore, M. D. Richardson, and R. H. Wilkens, "Exercising the Monte Carlo mine burial prediction system for impact and scour burial for operational Navy use," *IEEE J. Ocean. Eng.*, vol. 32, no. 1, pp. XXX–XXX, Jan. 2007.

[8] ***[AU: Please provide department]*** T. B. Smith, "Validation of the mine impact burial model using experimental data," M.S. thesis, Naval Postgrad. School, Monterey, CA, 2000.

[9] P. C. Chu, C. W. Fan, A. D. Evans, and A. F. Gilles, "Triple coordinate transforms for prediction of falling cylinder through the water column," *J. Appl. Mech.*, vol. 71, pp. 292–298, 2004.

[10] P. C. Chu, A. F. Gilles, C. W. Fan, J. Lan, and P. Fleischer, "Hydrodynamics of falling cylinder in water column," *Adv. Fluid Mech.*, vol. 4, pp. 163–181, 2002.

[11] P. C. Chu, A. F. Gilles, C. W. Fan, and P. Fleischer, "Hydrodynamics of falling mine in water column," in *Proc. 4th Int. Symp. Technol. Mine Problem*, 2000, CD-ROM.

[12] P. C. Chu and C. W. Fan, "Pseudo-cylinder parameterization for mine impact burial prediction," *J. Fluids Eng.*, vol. 127, pp. 1515–1520, 2005.

[13] ——, "Prediction of falling cylinder through air-water-sediment columns," *J. Appl. Mech.*, vol. 73, pp. 300–314, 2006.

[14] P. C. Chu, A. F. Gilles, and C. W. Fan, "Experiment of falling cylinder through the water column," *Exp. Thermal Fluid Sci.*, vol. 29, pp. 555–568, 2005.

[15] ***[AU: Please provide department]***A. Evans, "Hydrodynamics of mine impact burial," M.S. thesis, Monterey, CA, 2002.

[16] ***[Page range to come!]***C. P. Aubeny and H. Shi, "Effect of rate-dependent soil strength on cylinders penetrating into soft clay," *IEEE J. Ocean. Eng.*, vol. 32, no. 1, pp. XXX–XXX, Jan. 2007.

[17] P. C. Chu, C. W. Fan, and A. D. Evans, "Three-dimensional rigid body impact burial model (IMPACT35)," *Adv. Fluid Mech.*, vol. 6, pp. 43–52, 2004.

[18] P. C. Chu, A. Evans, T. Gilles, T. Smith, and V. Taber, "Development of Navy's 3D mine impact burial prediction model (IMPACT35)," in *Proc. 6th Int. Symp. Technol. Mine Problem*, Monterey, CA, 2004, DVD-ROM.

[19] ***[AU: This is the same reference as [13]. Please advise.]***P. C. Chu and C. W. Fan, "Prediction of falling cylinder through air-water-sediment columns," *J. Appl. Mech.*, vol. 73, pp. 300–314, 2006.

[20] ***[Page range to come!]***A. V. Abelev, P. J. Valent, and K. T. Holland, R. H. Wilkens and M. D. Richardson, Eds., "Behavior of a large cylinder in free fall through water," *IEEE J. Ocean. Eng.*, vol. 32, no. 1, pp. XXX–XXX, Jan. 2007.

[21] K. T. Holland, A. W. Green, A. Abelev, and P. J. Valent, "Parameterization of the in-water motions of falling cylinders using high-speed video," *Exp. Fluids*, vol. 37, pp. 690–770, 2004, doi: 10.1007/800348-004-0859-2.

[22] ***[AU: Please provide page range]***P. A. Elmore, R. Wilkens, T. Weaver, and M. D. Richardson, "IMPACT 28 and 35 simulations of 2003 Baltic Sea cruise: Model results and comparison with data," in *Proc. 5th Annu. ONR Workshop Mine Burial Prediction*, Kona, HI, Jan. 31– Feb. 2 2005.

[23] A. Palmer, "Speed effect in cutting and ploughing," *Geotechnique*, vol. 49, no. 3, pp. 285–294, 1997.

[24] B. C. Simonsen and N. E. O. Hansen, "Protection of marine structures by artificial islands," in *Ship Collision Analysis*, Gluver and Olsen, Eds. Rotterdam, The Netherlands: Balkema, 1998, pp. 201–215, ISBN: 9054109629.

[25] ***[AU: Please provide page range]***T. Wever, "Surprising mine burial observations at MVCO," in *Proc. 5th Annu. ONR Workshop Mine Burial Prediction*, Kona, HI, Jan. 31– Feb. 2 2005.

Peter C. Chu received the Ph.D. degree in geophysical fluid dynamics from the University of Chicago, Chicago, IL, in 1985.

He is a Professor of Oceanography and Head of the Naval Ocean Analysis and Prediction (NOAP) Laboratory, the Naval Postgraduate School, Monterey, CA. His research interests include ocean analysis and prediction, coastal modeling, littoral zone oceanography for mine warfare, mine impact burial prediction, mine acoustic detection, and satellite data assimilation for undersea warfare.

Chenwu Fan received the M.S. degree in mechanic engineering from China Textile University ***[AU: Please provide location of the university]*** in 1982.

He is an Oceanographer at the Naval Postgraduate School, Monterey, CA. His research interests include numerical simulation, ocean analysis and prediction, coastal modeling, littoral zone oceanography for mine warfare, and mine impact burial prediction.

Mine Impact Burial Model (IMPACT35) Verification and Improvement Using Sediment Bearing Factor Method

Peter C. Chu and Chenwu Fan

Abstract—**Recently, a 3-D model (IMPACT35) *[AU: If it is an acronym, please define]* was developed to predict a falling cylindrical mine's location and orientation in air–water–sediment columns. The model contains the following three components: 1) triple coordinate transform, 2) hydrodynamics of falling rigid object in a single medium (air, water, or sediment) and in multiple media (air–water and water–sediment interfaces), and 3) delta method for sediment resistance with the transient pore pressure. Two mine impact burial experiments were conducted to detect the mine trajectory in water column [Carderock Division, Naval Surface Warfare Center (NSWC), West Bethesda, MD, on September 10–14, 2001], and to measure the mine burial volume in sediment (Baltic Sea in June 2003). The existing IMPACT35 predicts mine's location and orientation in the water column, but not in the sediment column. Since sediment resistance largely affects the mine burial depth and orientation in sediment, a new method (bearing factor) is proposed to compute the sediment resistant force and torque. The improvement of IMPACT35 with the bearing factor method is verified using the data collected from the Baltic Sea mine impact burial experiment. The prediction error satisfies near-Gaussian distribution. The bias of the burial volume (in percent) prediction reduces from 11% using the delta method (old) to 0.1% using the bearing factor method (new). Correspondingly, the root mean square error (rmse) reduces from 26.8% to 15.8%.**

Index Terms—**Author, please supply your own keywords or send a blank e-mail to keywords@ieee.org to receive a list of suggested keywords.**

I. Introduction

THE conclusion of the cold war culminated with the Union of Soviet Socialist Republics (USSR) effectively ceasing to exist under international law on December 31, 1991. This historical event caused the U.S. military and specifically the U.S. Navy and Marine Corp Team to shift tactical emphasis from "blue" water, deep-ocean doctrine to littoral warfare doctrine. This shift predicated military responses dealing with a wide range of worldwide regional crises requiring forward sea basing, and expeditionary force landing support.

Sea mines are big threat in naval operations. Within the past 15 years three U.S. ships, the USS Samuel B. Roberts (FFG-58), Tripoli (LPH-10), and Princeton (CG-59) have fallen victim to mines. Total ship damage was $125 million while the mines cost approximately $30 000 [1]. Mines have evolved over the years from the dumb "horned" contact mines that damaged the Tripoli and Roberts to ones that are relatively sophisticated—nonmagnetic materials, irregular shapes, anechoic coatings, multiple sensors, and ship count routines. Despite their increased sophistication, mines remain inexpensive and are relatively easy to manufacture, keep, and place.

Accurate mine burial predictions are inherently difficult [2], [3] because of unknown conditions in mine deployment and uncertain environments such as waves, currents, and sediment transports [4]. The U.S. Navy developed operational models to forecast ocean environments for mine burial prediction [5], [6]. Recently, statistical methods such as the Monte Carlo [7] and the expert system methods [4] have been developed. These methods have a core-physical model for falling rigid body through air–water–sediment columns. The U.S. Navy has a 2-D model (IMPACT28) to predict cylinder's trajectory and impact burial. The data collected from the mine impact burial experiment in the surf zone near the Naval Postgraduate School, Monterey, CA, shows overprediction of the burial depth (an order of magnitude larger) using IMPACT28 [8].

A 3-D model (IMPACT35) was recently developed at the Naval Postgraduate School to predict cylinder's trajectory and impact burial [9]–[13]. The dynamical system can be simplified using the following three coordinate systems: earth-fixed coordinate (E-coordinate), cylinder's main axis following coordinate (M-coordinate), and hydrodynamic force following coordinate (F-coordinate). The origin of both M- and F-coordinates is at the cylinder's center of mass (COM). The body forces and their moments are easily calculated using the E-coordinate system. The hydrodynamic forces and their moments are easily computed using the F-coordinate. The cylinder's moments of gyration are simply represented using the M-coordinate. When the mine penetrates into an interface between two media (air–water or water–sediment), the cylinder is decomposed into two parts with each one contacting one medium. The body forces (such as the buoyancy force) and surface forces (such as pressure, hydrodynamic force) are computed separately for the two parts. A fully 3-D model is developed for predicting the translation velocity and orientation of a falling cylindrical

Manuscript received March 28, 2005; revised May 19, 2006; accepted August 8, 2006. This work was supported by the U.S. Office of Naval Research Marine Geosciences Program N0001403WR20178 and N0001404WR20067, by the Naval Oceanographic Office, and by the Naval Postgraduate School. **Guest Editor: M. D. Richardson**.

The authors are with the Naval Ocean Analysis and Prediction Laboratory, Department of Oceanography, Naval Postgraduate School, Monterey, CA 93943 USA (e-mail: pcchu@nps.edu).

Color versions of one or more of the figures in this paper are available online at http://ieeexplore.ieee.org.

Digital Object Identifier 10.1109/JOE.2007.890942

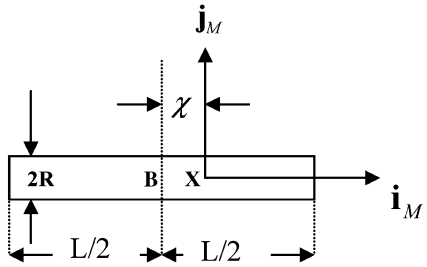

Fig. 1. M-coordinate with the COM as the origin $\mathbf{X}$ and (i_m, j_m) as the two axes. Here, χ is the distance between the COV $(\mathbf{B})$ and COM $(\mathbf{X})$; (L, R) are the cylinder's length and radius.

mine through air, water, and sediment. The value-added capability of the 3-D model (IMPACT35) versus the 2-D model (IMPACT28) is verified using experimental data.

Recently, two mine impact burial experiments were conducted to detect mine trajectory in the water column [Carderock Division, Naval Surface Warfare Center (NSWC), West Bethesda, MD, on September 10–14, 2001] and to measure the mine burial in the sediment (Baltic Sea in June 2003). The collected data are used for model verification. Section II describes basic physics of the recently developed 3-D model (IMPACT35). Section III shows the value-added ***[AU: Change to "added value" throughout?]*** of IMPACT35 in predicting mine movement in water column. However, Section IV shows weakness of the existing IMPACT35 in predicting mine movement in sediment. Section V presents the new bearing factor method to compute the sediment resistant force and torque. Section VI shows the improvement of the bearing factor method in predicting mine burial in sediment. Section VII presents the conclusions.

II. Description of IMPACT35

The 3-D mine impact burial prediction model (IMPACT35) contains the following major components: 1) triple coordinate systems, 2) momentum balance, 3) moment of momentum balance, 4) hydrodynamics, and 5) sediment dynamics. Among them, the hydrodynamics (drag and lift forces and torques) have been described in [9] and [12]–[14], and will not be discussed here.

A. Triple Coordinate Systems

Consider an axially symmetric cylinder with the center of mass (COM) $\mathbf{X}$ and the center of volume (COV) $\mathbf{B}$ on the main axis (Fig. 1). Let (L, R, χ) represent the cylinder's length, radius, and the distance between the two points $(\mathbf{X}, \mathbf{B})$. The positive χ-values refer to nose-down case, i.e., the point $\mathbf{X}$ is lower than the point $\mathbf{B}$. Three coordinate systems are used to model the falling cylinder through the air, water, and sediment phases: earth-fixed coordinate (E-coordinate), main axis following coordinate (M-coordinate), and force following coordinate (F-coordinate) systems. All the systems are 3-D, orthogonal, and right-handed [9].

The E-coordinate system is represented by $F_E(O, \mathbf{i}, \mathbf{j}, \mathbf{k})$ with the origin O, and three axes: x- and y-axes (horizontal)

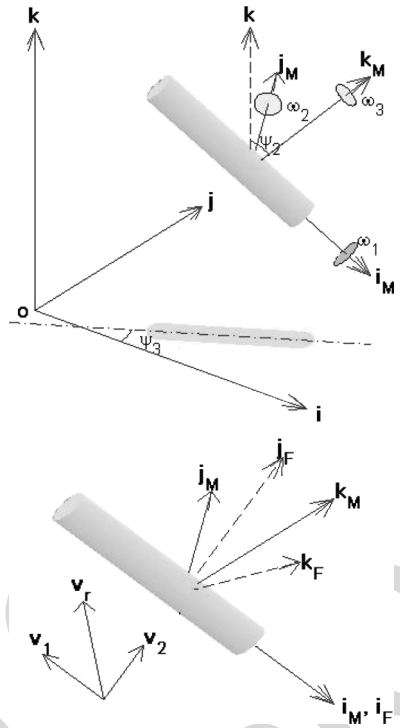

Fig. 2. Three coordinate systems. Here, $(\mathbf{i}, \mathbf{j}, \mathbf{k})$ are the unit vectors of E-coordinate system. Both M- and F-coordinate systems share the same axis, i.e., $\mathbf{i}_M$ and $\mathbf{i}_F$ are the same unit vectors.

with the unit vectors $(\mathbf{i}, \mathbf{j})$ and z-axis (vertical) with the unit vector $\mathbf{k}$ (upward positive). The position of the cylinder is represented by the position of the COM

$$\mathbf{X} = x\mathbf{i} + y\mathbf{j} + z\mathbf{k} \tag{1}$$

which describes translation of the cylinder. The translation velocity is given by

$$\frac{d\mathbf{X}}{dt} = \mathbf{V}, \qquad \mathbf{V} = (u, v, w). \tag{2}$$

Let the orientation of the cylinder's main axis (pointing downward) be given by $\mathbf{i}_M$. The angle between $\mathbf{i}_M$ and $\mathbf{k}$ is denoted by $\psi_2 + \pi/2$. Projection of the vector $\mathbf{i}_M$ onto the (x, y)-plane creates angle (ψ_3) between the projection and the x-axis (Fig. 2). The M-coordinate system is represented by $F_M(\mathbf{X}, \mathbf{i}_M, \mathbf{j}_M, \mathbf{k}_M)$ with the origin $\mathbf{X}$, unit vectors $(\mathbf{i}_M, \mathbf{j}_M, \mathbf{k}_M)$, and coordinates (x_M, y_M, z_M). In the plane consisting of vectors $\mathbf{i}_M$ and $\mathbf{k}$ (passing through the point M), two new unit vectors $(\mathbf{j}_M, \mathbf{k}_M)$ are defined with $\mathbf{j}_M$ perpendicular to the $(\mathbf{i}_M, \mathbf{k})$-plane, and $\mathbf{k}_M$ perpendicular to $\mathbf{i}_M$ in the $(\mathbf{i}_M, \mathbf{k})$-plane. The unit vectors of the M-coordinate system are given by (Fig. 2)

$$\mathbf{j}_M = \mathbf{k}_M \times \mathbf{i}_M, \quad \mathbf{k}_M = \mathbf{i}_M \times \mathbf{j}_M. \tag{3}$$

The M-coordinate system is solely determined by orientation of the cylinder's main axis $\mathbf{i}_M$.

The F-coordinate system is represented by $F_F(\mathbf{X}, \mathbf{i}_F, \mathbf{j}_F, \mathbf{k}_F)$ with the origin $\mathbf{X}$, unit vectors

TABLE I
PHYSICAL PARAMETERS OF THE MODEL MINES IN THE NSWC-CARDEROCK EXPERIMENT (AFTER [20])

Mine	Mass (kg)	ρ (10^3 kg m^{-3})	L (m)	J_1 (kg m^2)	J_2 (J_3) (kg m^2)	χ (m)
1	16.96	1.60	0.505	0.0647	0.356	0
2	22.27	2.10	0.505	0.0806	0.477	0
3	34.93	1.60	1.010	0.1362	2.900	0
4	45.85	2.10	1.010	0.1696	3.820	0
5	45.85	2.10	1.010	0.1693	3.940	0.0045
6	45.85	2.10	1.010	0.1692	4.570	-0.077

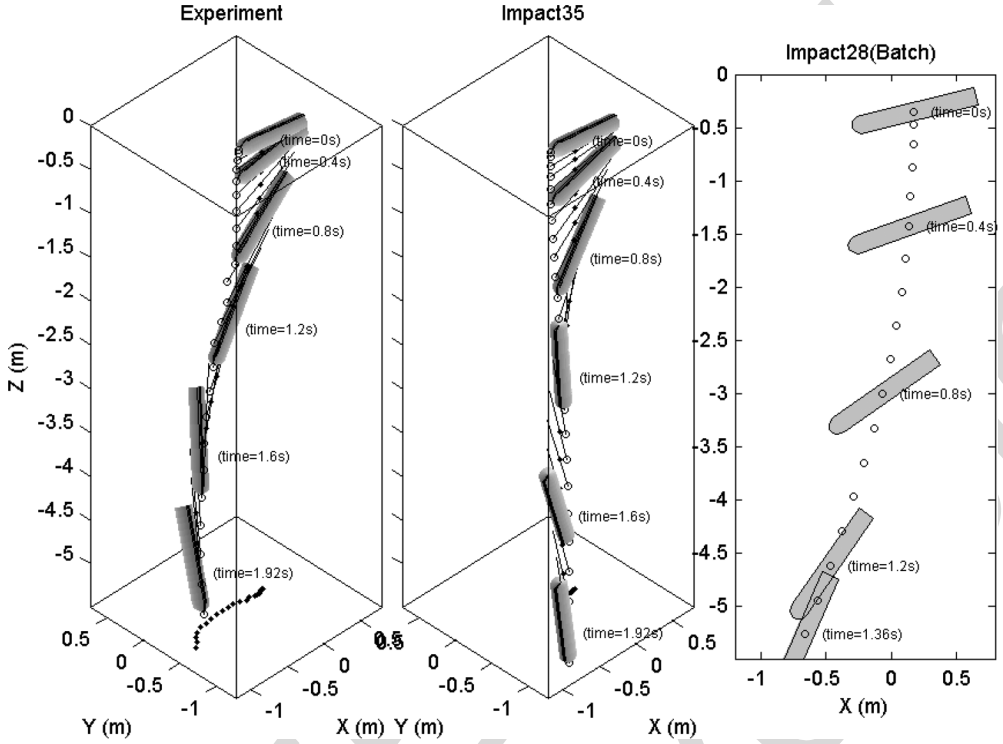

Fig. 3. Movement of mine #6 ($L = 1.01$ m, $\rho = 2.1 \times 10^3$ kg m^{-3}) with $\chi = -0.0077$ m and $\psi_2 = -14.0°$ obtained from (a) NSWC-Carderock experiment, (b) 3-D IMPACT35 model, and (c) 2-D IMPACT28 model. **AU: Please add space between number and unit in Figs. 3, 4, 5.**

$(\mathbf{i}_F, \mathbf{j}_F, \mathbf{k}_F)$, and coordinates (x_F, y_F, z_F). Let $\mathbf{V}_w$ be the fluid velocity. The fluid-to-cylinder velocity is represented by $\mathbf{V}_r = \mathbf{V}_w - \mathbf{V}$, that is decomposed into two parts

$$\mathbf{V}_r = \mathbf{V}_1 + \mathbf{V}_2 \quad \mathbf{V}_1 = V_1 \mathbf{i}_F \quad \mathbf{V}_2 = V_2 \mathbf{j}_F \tag{4}$$

where

$$\mathbf{V}_1 = (\mathbf{V}_r \cdot \mathbf{i}_F)\mathbf{i}_F$$

is the component paralleling to the cylinder's main axis (i.e., along $\mathbf{i}_M$), and

$$\mathbf{V}_2 = \mathbf{V}_r - (\mathbf{V}_r \cdot \mathbf{i}_F)\mathbf{i}_F$$

is the component perpendicular to the cylinder's main-axial direction. The unit vectors for the F-coordinate are defined by (column vectors)

$$\mathbf{i}_F = \mathbf{i}_M = \begin{bmatrix} r_{11} \\ r_{21} \\ r_{31} \end{bmatrix} \quad \mathbf{j}_F = \mathbf{V}_2/|\mathbf{V}_2| \quad \mathbf{k}_F = \mathbf{i}_F \times \mathbf{j}_F. \tag{5}$$

The F-coordinate system is solely determined by orientation of the cylinder's main axis $(\mathbf{i}_M)$ and the water-to-cylinder velocity. Note that the M- and F-coordinate systems have one common unit vector $\mathbf{i}_M$ (orientation of the cylinder). Use of the F-coordinate system simplifies the calculations for the lift and drag forces and torques acting on the cylinder.

B. Momentum Balance

The 3-D translation velocity of the cylinder $(\mathbf{V})$ is governed by the momentum equation in the E-coordinate system [9], [12]–[14]

$$\frac{d}{dt}\begin{bmatrix} u \\ v \\ w \end{bmatrix} = -\begin{bmatrix} 0 \\ 0 \\ g \end{bmatrix} + \frac{\mathbf{F}_{nh} + \mathbf{F}_h}{\rho \Pi} \tag{6}$$

where g is the gravitational acceleration, Π is the cylinder volume, ρ is the rigid body density, $\rho\Pi = m$ is the cylinder mass, $\mathbf{F}_{nh}$ is the nonhydrodynamic force defined later, and $\mathbf{F}_h$ is the hydrodynamic force (i.e., surface force including drag, lift forces). Both $\mathbf{F}_{nh}$ and $\mathbf{F}_h$ are integrated for the cylinder. The drag and lift forces are calculated using the drag and lift

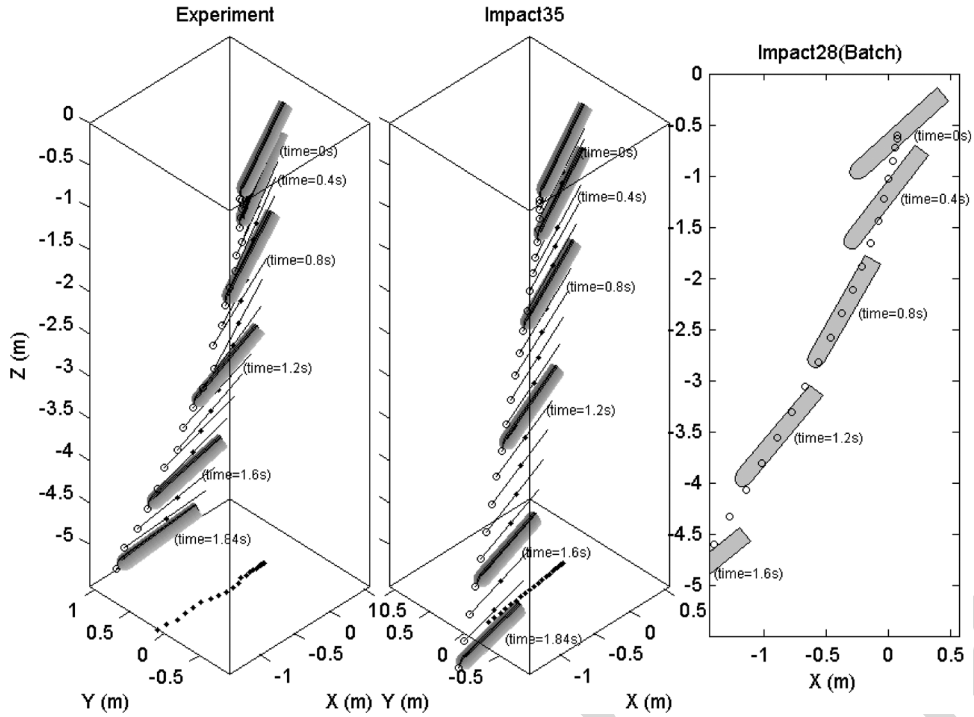

Fig. 4. Movement of mine #5 ($L = 1.01$ m, $\rho = 2.1 \times 10^3$ kg m^{-3}) with $\chi = 0.0045$ m and $\psi_2 = 42.2°$ obtained from (a) NSWC-Carderock experiment, (b) 3-D IMPACT35 model, and (c) 2-D IMPACT28 model.

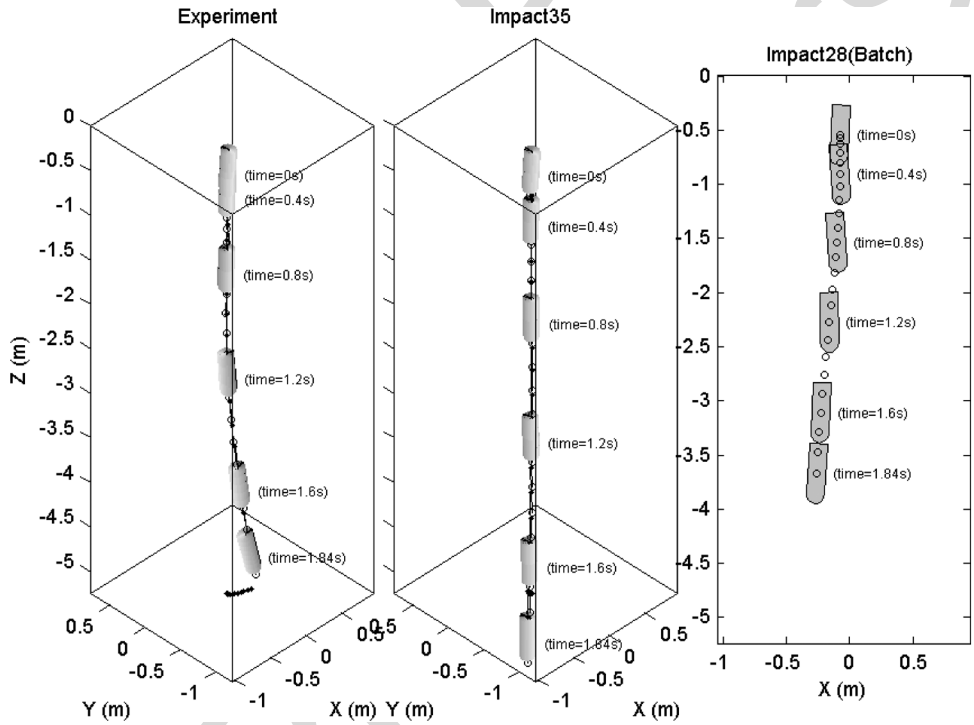

Fig. 5. Movement of mine #2($L = 0.505$ m, $\rho = 2.1 \times 10^3$ kg m^{-3}) with $\chi = 0$ and $\psi_2 = 87.0°$ obtained from (a) NSWC-Carderock experiment, (b) 3-D IMPACT35 model, and (c) 2-D IMPACT28 model.

laws with the given water-to-cylinder velocity $(\mathbf{V}_r)$. In the F-coordinate, $\mathbf{V}_r$ is decomposed into along-cylinder $(\mathbf{V}_1)$ and across-cylinder $(\mathbf{V}_2)$ components. The nonhydrodynamic force $\mathbf{F}_{nh}$ is the buoyancy force $(\mathbf{F}_b)$ for the air and water phases

$$\mathbf{F}_{nh} = \mathbf{F}_b = \mathbf{k}(\rho_a \Pi g, \rho_w \Pi g) \tag{7}$$

where (ρ_a, ρ_w) are the air and water densities and $\mathbf{F}_{nh}$ is the resultant of buoyancy force $(\mathbf{F}_b)$, and shearing resistance force $(\mathbf{F}_s)$ for the sediment phase.***[AU: Eq. (9) followed (7) in the original. It was changed to (8) and all following eq. numbers were changed accordingly. Please check.]***

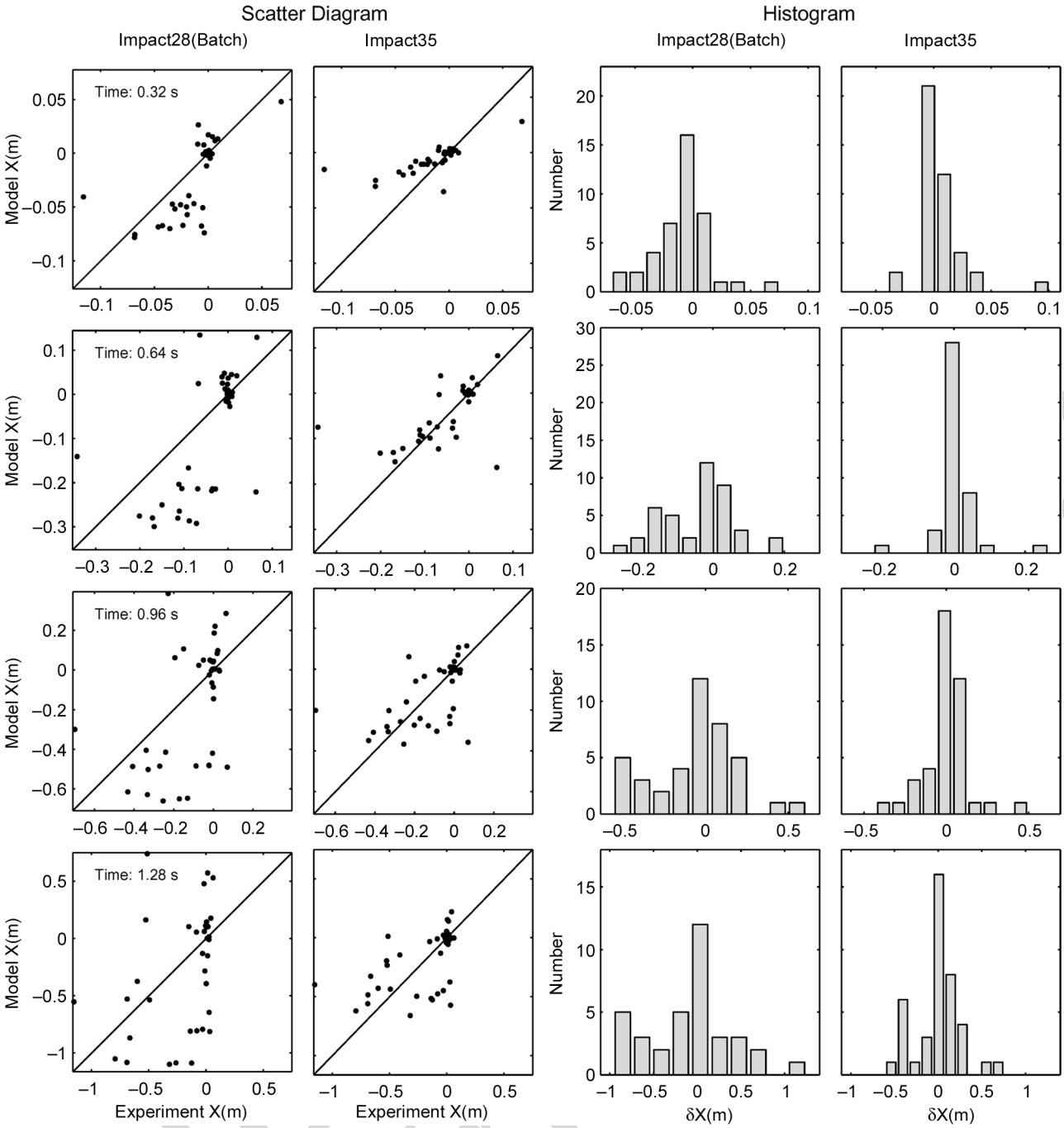

Fig. 6. Model verification from prediction of the COM position x using the NSWC-Carderock experiment data at several time instances: 0.32, 0.64, 0.96, and 1.28 s. Here, the first column is the data-IMPACT28 comparison, the second column is the data-IMPACT35 comparison, the third column shows the histograms of the model error (δx) for IMPACT28, and the fourth column shows the histograms of the model error (δx) for IMPACT35.

C. Moment of Momentum Equation

The moment of momentum equation is written in the M-coordinate system, which rotates with the angular velocity of

$$\mathbf{\Omega} = \omega_2 \mathbf{j}_M + \omega_3 \mathbf{k}_M. \tag{8}$$

Usually, the angular velocity around the mine's main axis $\mathbf{i}_M$ (i.e., self-spinning velocity) is very small $(\omega_1 \simeq 0)$ and neglected. Thus, we have

$$\mathbf{\Omega} = \boldsymbol{\omega}.$$

This leads to zero centripetal and "Coriolis" terms

$$\mathbf{\Omega} \times (\mathbf{\Omega} \times \boldsymbol{\omega}) = 0 \quad -2\mathbf{J} \bullet (\mathbf{\Omega} \times \boldsymbol{\omega}) = 0. \tag{9}$$

The inertial term

$$\frac{d\mathbf{\Omega}}{dt} \times \boldsymbol{\omega} = \mathbf{i}_M \left(\omega_3 \frac{d\omega_2}{dt} - \omega_2 \frac{d\omega_3}{dt} \right) \tag{10}$$

only has the component along the direction of $\mathbf{i}_M$ (mine's main axis). This term may be neglected when the self-spinning

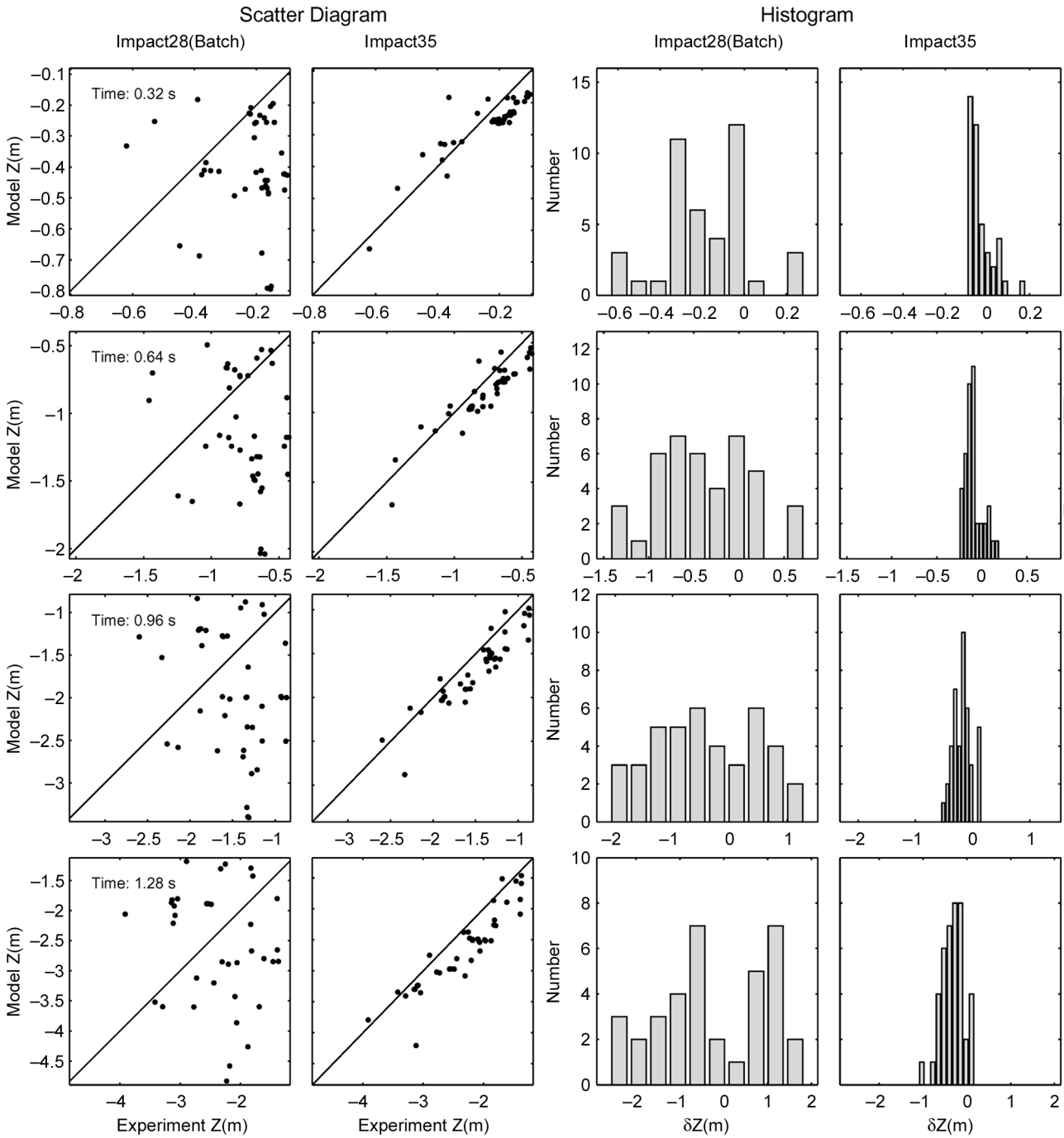

Fig. 7. Model verification from prediction of the COM position z using the NSWC-Carderock experiment data at several time instances: 0.32, 0.64, 0.96, and 1.28 s. Here, the first column is the data-IMPACT28 comparison, the second column is the data-IMPACT35 comparison, the third column shows the histograms of the model error (δx) for IMPACT28, and the fourth column shows the histograms of the model error (δx) for IMPACT35.

velocity is small. The moment of momentum equation in the M-coordinate system can be simplified by

$$\mathbf{J} \bullet \frac{d\boldsymbol{\omega}}{dt} \simeq \mathbf{M}_{nh} + \mathbf{M}_h \tag{11}$$

where $\mathbf{M}_{nh}$ and $\mathbf{M}_h$ are the nonhydrodynamic and hydrodynamic force torques. In the M-coordinate system, the moment of gyration tensor for the axially symmetric cylinder is a diagonal matrix

$$\mathbf{J} = \begin{bmatrix} J_1 & 0 & 0 \\ 0 & J_2 & 0 \\ 0 & 0 & J_3 \end{bmatrix} \tag{12}$$

where J_1, J_2, and J_3 are the moments of inertia. The nonhydrodynamic force usually contains the gravity and buoyancy forces.

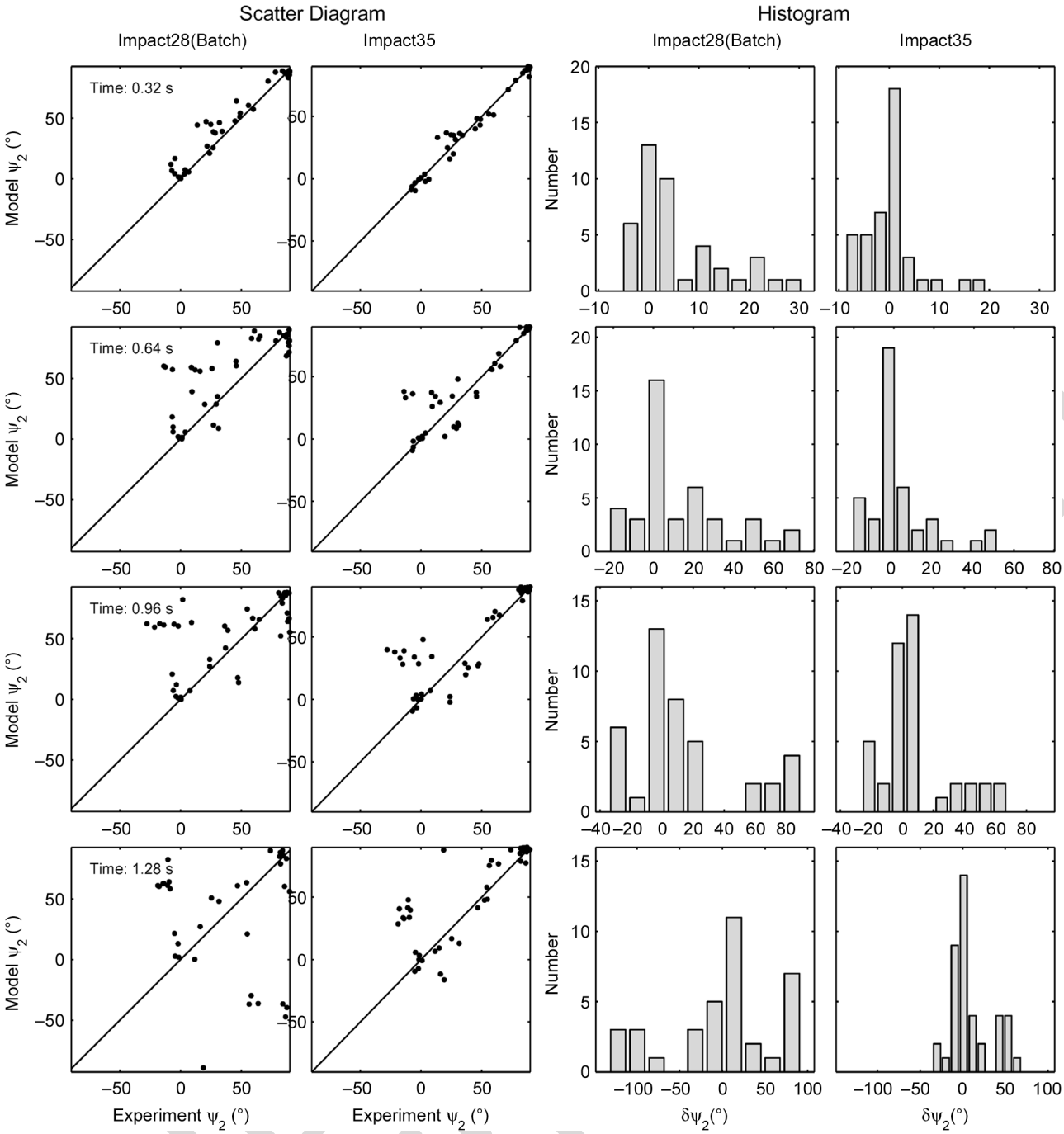

Fig. 8. Model verification from prediction of the orientation ψ_2 using the NSWC-Carderock experiment data at several time instances: 0.32, 0.64, 0.96, and 1.28 s. Here, the first column is the data-IMPACT28 comparison, the second column is the data-IMPACT35 comparison, the third column shows the histograms of the model error $(\delta\psi_2)$ for IMPACT28, and the fourth column shows the histograms of the model error $(\delta\psi_2)$ for IMPACT35.

The gravity force, passing the COM, does not induce the moment. The buoyancy force induces the moment in the $\mathbf{j}_M$ direction if the COM does not coincide with the COV (i.e., $\chi \neq 0$)

$$\mathbf{M}_b = |\mathbf{F}_b|\chi \cos\psi_2 \mathbf{j}_M. \tag{13}$$

D. Sediment Dynamics

In the existing IMPACT35 model, the sediment resistance is calculated using the delta method. This method is on the base on the assumption that the cylinder pushes the sediment and leaves space in the wake as it impacts and penetrates into the sediment. This space is refilled by water and the water cavity is produced. At the instance of the penetration, the total resistant force on the cylinder is represented by [17]–[19]

$$\mathbf{F}^s = \int_{\sigma_{\text{sed}}} \left[\delta\left(\mathbf{f}_b^s + \mathbf{f}_{sh}\right) + \mathbf{f}_b^w + \mathbf{f}_h^w\right] d\sigma + \mathbf{F}_{pw} \tag{14}$$

where $(\mathbf{f}_b^s, \mathbf{f}_{sh})$ and $(\mathbf{f}_b^w, \mathbf{f}_h^w)$ are the sediment buoyancy and shear resistance forces and water buoyancy and hydrodynamic forces (per unit area) at the point $\mathbf{r}$ over the cylinder's surface,

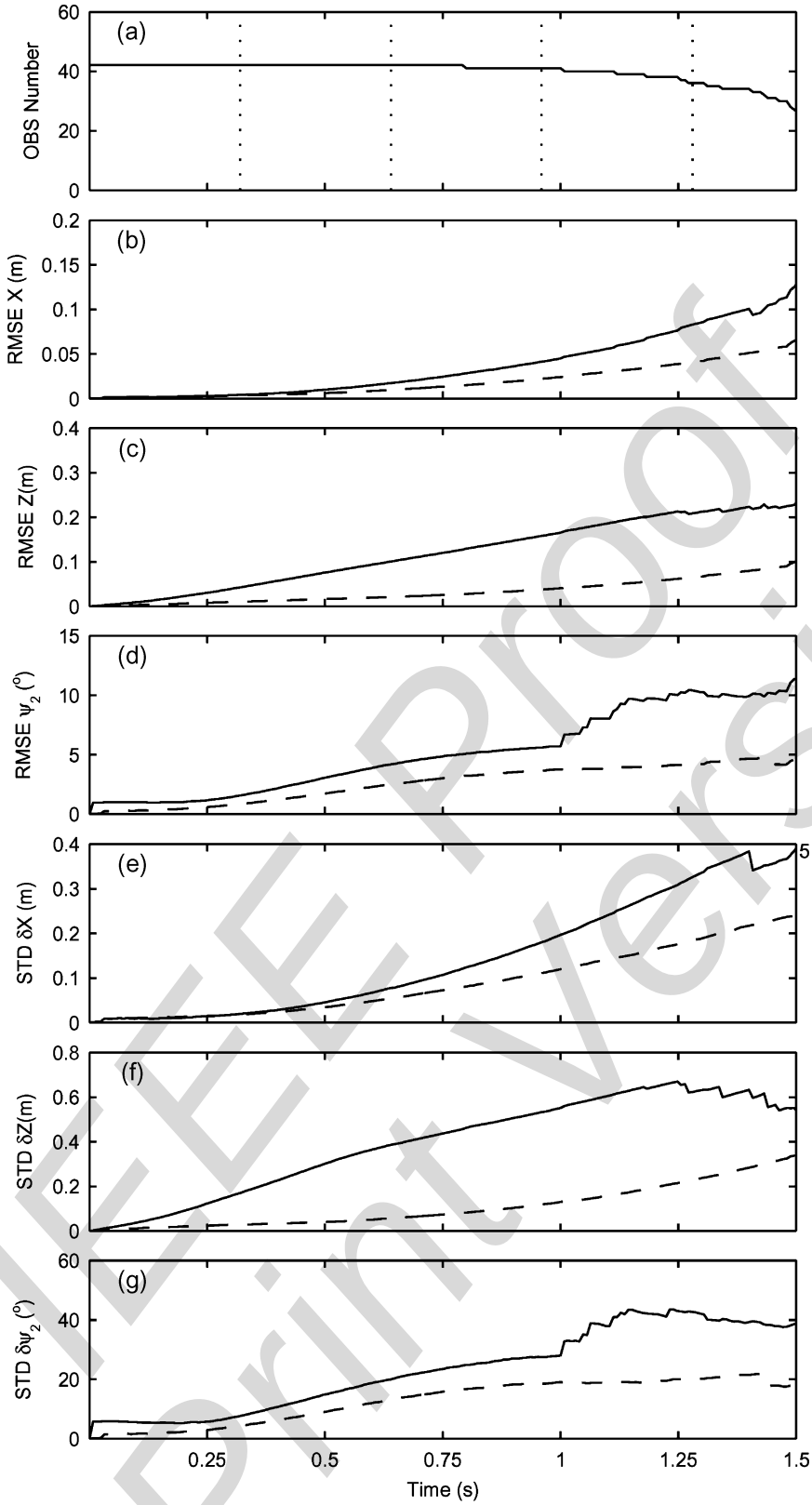

Fig. 9. Temporal evolution of model performance evaluated using the NSWC-Carderock data: (a) observational data number, (b) rmse of x, (c) rmse of z, (d) rmse of ψ_2, (e) STD of δx, (f) STD of δz, and (g) STD of $\delta\psi_2$ with the solid curves for IMPACT35 and dashed curves for IMPACT28 from (b) to (g). **AU: Please change "RMSE" to "rmse" as per IEEE style.**

Fig. 10. Optical mine used in the Baltic Sea experiment (after [25]).

TABLE II
PHYSICAL PARAMETERS OF THE FULL-SIZE OPTICAL MINE IN THE BALTIC SEA EXPERIMENT (AFTER [25])

Length (m)	1.466
Diameter (m)	0.470
Taper Diameter (m)	0.395
Taper Length (m)	0.150
Volume (m^3)	0.252
Mass (kg)	550.00
χ (m)	0
J_1 (kg m^2)	14.82
J_2, J_3 (kg m^2)	105.00

TABLE III
PHYSICAL PARAMETERS OF THE ENVIRONMENT IN THE BALTIC SEA EXPERIMENT (AFTER [25])

Air Density (kg m^{-3})	1.22
Water Density (kg m^{-3})	1025.8
Air Kinetic Viscosity (m^2 s^{-1})	1.46×10^{-5}
Water Kinetic Viscosity (m^2 s^{-1})	1.13×10^{-6}

σ_{sed} is the area of the cylinder's surface below the water–sediment interface, $\mathbf{F}_{pw}$ is the pore water pressure force on the whole cylinder, and δ-function is defined by

$$\delta = \begin{cases} 1 & \mathbf{v} \bullet \mathbf{n} \geq 0 \\ 0 & \mathbf{v} \bullet \mathbf{n} \leq 0 \end{cases} \tag{15}$$

which shows that the sediment buoyancy and shear resistance forces act when the cylinder moves towards them. Here, $\mathbf{v}$ is the velocity at point $\mathbf{r}$ (represented in the M-coordinate) on the cylinder surface

$$\mathbf{v} = \mathbf{V} + \boldsymbol{\omega} \times \mathbf{r}. \tag{16}$$

III. VERIFICATION OF IMPACT35 IN THE WATER COLUMN

The NSWC–Carderock experiment was conducted on September 10-14, 2001 in the Explosion Test Pond, which is the only explosive-related test pond in the United States with the capability of providing high-speed underwater photography given its exceptional water clarity. In addition, the facility concrete floor thickness and reinforcement is sufficient to allow impact of 45-kg cylinders without additional floor protection. The pond in plan view is a regular pentagon with each side of 41 m. During the experiment, six model mines (Table I) with mass varying from 16.96 to 45.85 kg were released to the pond with the water depth at 7.92 m [20], [21]. The data set collected from the NSWC-Carderock experiment was used to evaluate value-added of IMPACT35 versus IMPACT28 (2-D model).

A. Near Horizontal Release

Model mine #6 was released to the water with $\psi_2 = -14°$ (near horizontal, see Fig. 2). The physical parameters of this mine are given by

$$\begin{aligned} &L{=}1.01\text{ m} \quad \rho{=}2.10\times10^3\text{ kg m}^{-3} \quad \chi{=}-0.077\text{ m} \\ &m{=}45.85\text{ kg} \quad J_1{=}0.1692\text{ kg m}^2 \quad J_2{=}J_3{=}4.570\text{ kg m}^2. \end{aligned} \tag{17}$$

The initial conditions are given by

$$\begin{aligned} &x_0 = y_0 = z_0 = 0 \quad u_0 = v_0 = w_0 = 0 \\ &r\psi_{10} = 0 \quad \psi_{20} = -14° \quad \psi_{30} = 0 \quad \omega_{10} = \omega_{20} = \omega_{30} = 0. \end{aligned} \tag{18}$$

Substitution of the model parameters (17) and the initial conditions (18) into IMPACT28 and IMPACT35 leads to the prediction of the mine's translation and orientation that are compared with the data collected during the experiment at each time step (Fig. 3). The new 3-D model (IMPACT35) simulated trajectory agrees well with the observed trajectory. Both show the same pattern and the same travel time (1.92 s) for the cylinder passing through the water column. However, the 3-D model (IMPACT35) is better than the 2-D model (IMPACT28) in predicting the mine's movement in the water column.

B. Near 45° Release

Model mine #6 was released to the water with $\psi_2 = 42.2°$. The initial conditions are given by

$$\begin{aligned} &x_0{=}y_0{=}z_0{=}0 \quad u_0{=}v_0{=}w_0{=}0 \\ &\psi_{10}{=}0 \quad \psi_{20}{=}42.2° \quad \psi_{30}{=}0 \quad \omega_{10}{=}\omega_{20}{=}\omega_{30}{=}0. \end{aligned} \tag{19}$$

Substitution of the model parameters (17) and the initial conditions (19) into IMPACT28 and IMPACT35 leads to the prediction of the mine's translation and orientation that are compared with the data collected during the experiment at time steps (Fig. 4). Both 3-D model (IMPACT35) and 2-D model (IMPACT28) simulated trajectories and travel times agree well with the observed trajectory.

C. Near Vertical Release

Model mine #2 was released to the water with $\psi_2 = 87°$. The physical parameters of this mine are given by

$$\begin{aligned} &L = 0.505\text{ m} \quad \rho = 2.10\times10^3\text{ kg m}^{-3} \quad \chi = 0 \\ &m = 22.27\text{ kg} \quad J_1 = 0.0806\text{ kg m}^2 \\ &J_2 = J_3 = 0.477\text{ kg m}^2. \end{aligned} \tag{20}$$

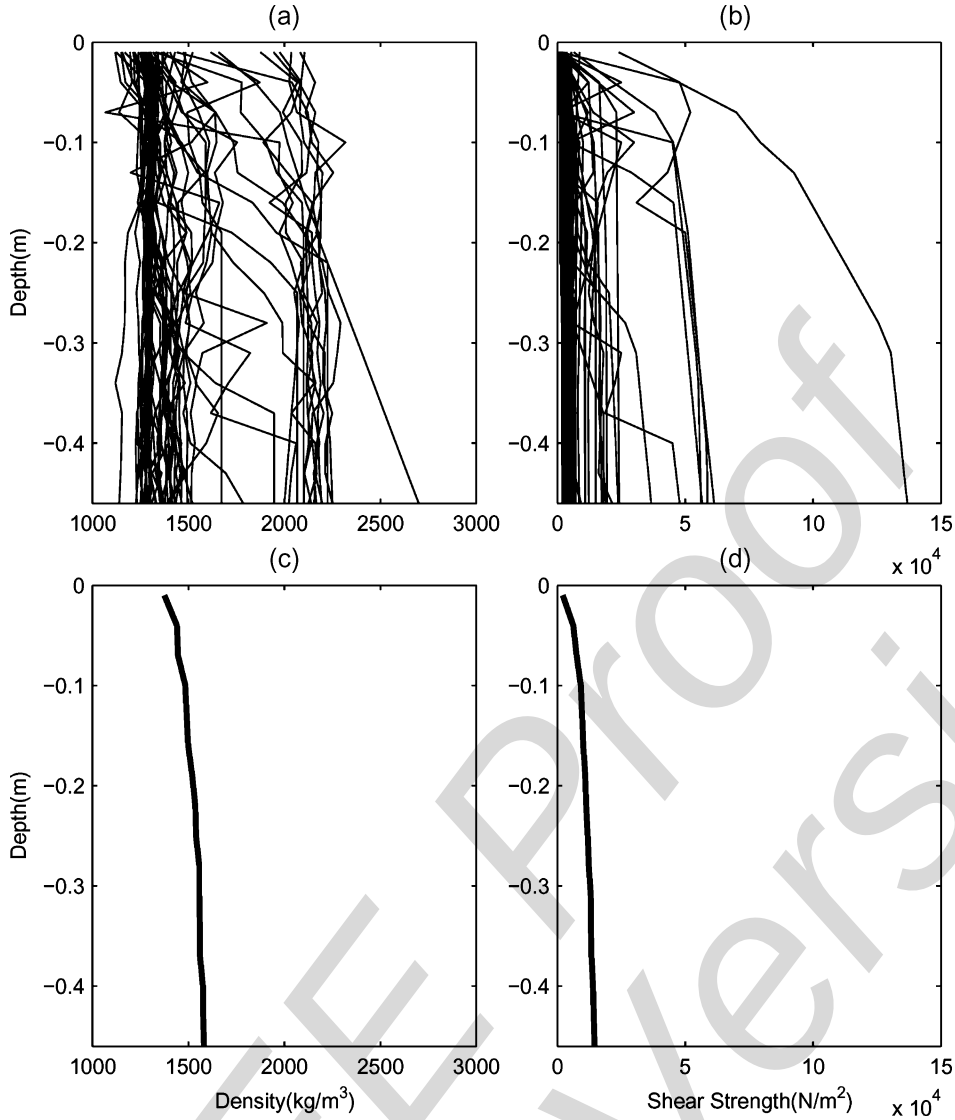

Fig. 11. Sediment density $\rho_s(z)$ and static shear strength $S(z)$ profiles in the Baltic Sea from the cores collected at 59 mine impact sites during the mine-drop experiment in June 2003: (a) individual density profiles, (b) individual static shear strength profiles, (c) mean density profile, and (d) mean static shear strength profile (after [25]). **AU: Should "kg/m^3" be "kg m^3" and "N/m^2" " N m^2 ? If yes, please provide new figure.**

The initial conditions are given by

$$x_0 = y_0 = z_0 = 0 \quad u_0 = v_0 = w_0 = 0$$
$$\psi_{10} = 0 \quad \psi_{20} = 87^\circ \quad \psi_{30} = 0 \quad \omega_{10} = \omega_{20} = \omega_{30} = 0. \quad (21)$$

The predicted cylinder's translation and orientation are compared with the data collected at time steps (Fig. 5). The 3-D model (IMPACT35) simulated trajectory agrees well with the observed trajectory. Both show the same straight pattern and the same travel time (1.84 s) for the cylinder passing through the water column.

D. Statistical Error Analysis

Figs. 6–8 show scatter diagrams and histograms for predicting mine's location and orientation $[x(t), z(t), \psi_2(t)]$. In the scatter diagrams, the points cluster around the diagonal line of $\varsigma_m = \varsigma_o$ using IMPACT35 (second column), and the points are spreading out of the diagonal line using IMPACT28 (first column), which confirms that IMPACT35 predicts COM position more accurately than IMPACT28. Histograms of model errors for COM position have Gaussian-type distribution with near-zero mean and small standard deviation (STD) using IMPACT35 (fourth column), and non-Gaussian-type distributions with large STD using IMPACT28 (third column).

The total number of observational points at each time instance $N(t)$ is around 41 as t <1.2 s and reduces quickly with time as t >1.2 s Fig. 9(a), which indicates that the model verification is reliable for t <1.2 s. The value-added of IMPACT35 is easily seen from Fig. 9. For example, the root mean square error (rmse) of COM prediction is much smaller when using IMPACT35 than IMPACT28 [Fig. 9(b) and (c)]. The STDs of the model errors for the COM prediction are also much lower when using IMPACT35 than IMPACT28 [Fig. 9(e) and (f)]. The rmse of orientation prediction is smaller when using IMPACT35 than IMPACT28 for t <1 s. When t >1 s, the rmse

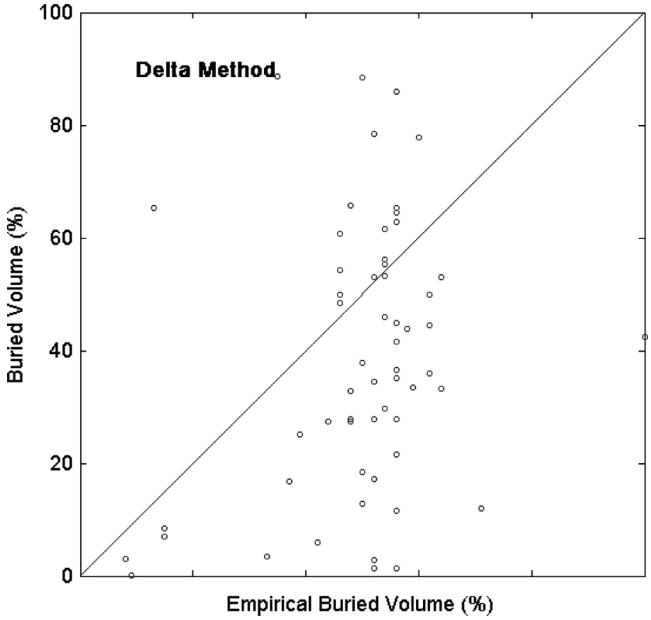

Fig. 12. Scatter diagrams of buried volume prediction against the Baltic Sea experimental data. Here, IMPACT35 uses the delta method for sediment resistance.

of ψ_2 is around half when using IMPACT35 than when using IMPACT28 [Figs. (9d) and (g)].

IV. Verification of IMPACT35 in Sediment

The Baltic Sea experiment was conducted in June 2003 by the German Federal Armed Forces Underwater Acoustic and Marine Geophysics Research Institute (FWG, Kiel, Germany) [22] with the full-size optical mine (Fig. 10) which is allowed to free fall from the wench. Table II shows the physical parameters of the optical mine. Table III lists the physical environments in the Baltic Sea. The full-size optical mine was released 59 times. The water depths of the drop sites were between 25.0 and 26.5 m (Fig. 11). The volume of mine burial percentage was measured. The readers are referred to [7] for detailed information.

After running IMPACT35 with the delta method for the sediment resistance (14) for each gravity core regime $[\rho_s(z), S(z)]$, the predicted and observed burial volumes (in percent) were compared (Fig. 12). The bias (mean predicted minus observed values) and rmse of burial volume are 11% and 26.8%. The correlation coefficient between predicted and observed burial volumes is 0.374%.

The histograms of the burial volume (in percent) are very different between the Baltic Sea experiment and the model prediction of IMPACT35 using the delta method [Fig. 13(a) and (b)]. In the experiment, the probability density function (pdf) has a peak at burial volume of 50% with a frequency of 26. However, the model predicted pdf has a peak at 30% with a frequency of 11.

V. Bearing Factor Method

New (bearing factor) method is presented for calculating the sediment resistant force and torque.

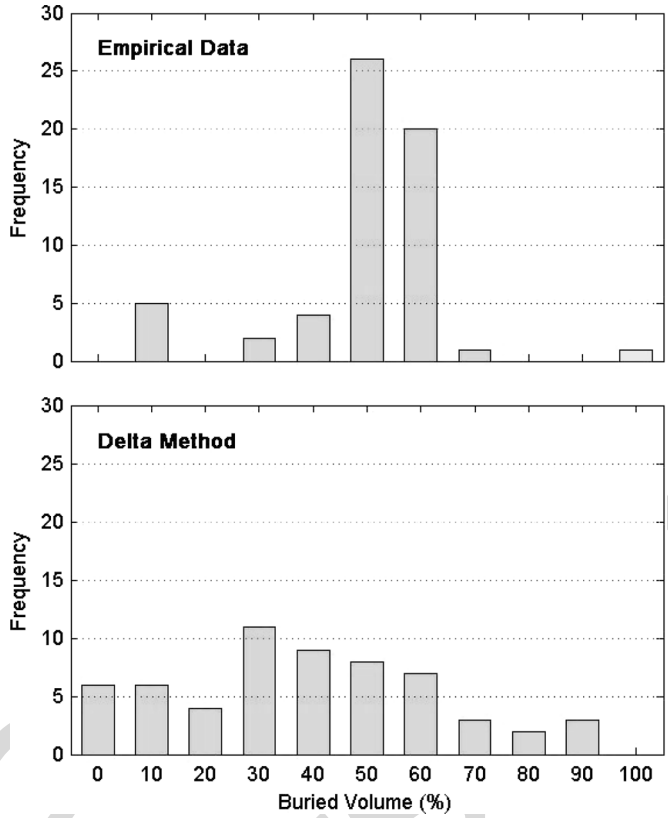

Fig. 13. Histograms of buried volume (in percent) from (a) Baltic Sea experiment and (b) prediction using IMPACT35 with the delta method.

A. Sediment Resistance

When the mine impacts and penetrates into the sediment, it creates a large transient pore pressure in the sediment that causes ruptures in the sediment and influences the resistance force on the cylinder [23], [24]. The resistance of the sediment to mine's penetration is assumed to have the following three components: buoyancy force $\mathbf{F}_b^s$, hydrodynamic (drag and lift) force $\mathbf{F}_h^s$ (similar to air and water), and shear resistance force $\mathbf{F}_r^S$ (resistance to the rupture)

$$\mathbf{F}^s = \mathbf{F}_b^s + \mathbf{F}_h^s + \mathbf{F}_r^s. \tag{22}$$

The sediment buoyancy force per unit area is defined by

$$\mathbf{F}_b^s = -\mathbf{n} \int_z^{z_{ws}} \rho_s(z') g dz' \tag{23}$$

where $\rho_s(z)$ is the sediment wet density (usually obtained from the sediment data), $\mathbf{n}$ is unit vector normal to the mine surface (outward positive), and z_{ws} represents the vertical coordinate of the water–sediment interface.

The shear resistance force $(\mathbf{F}_r^S)$ is in the opposite direction of $\mathbf{v}$ and acts on the mine. Its magnitude is proportional to the product of the sediment shear strength (S) and the rupture area (A, projection of sediment-contacting area perpendicular to the velocity $\mathbf{V}$) with a nonnegative bearing factor N [16]

$$\mathbf{F}_r^s = -\boldsymbol{\tau} N(p, v) S A, \qquad N \geq 0. \tag{24}$$

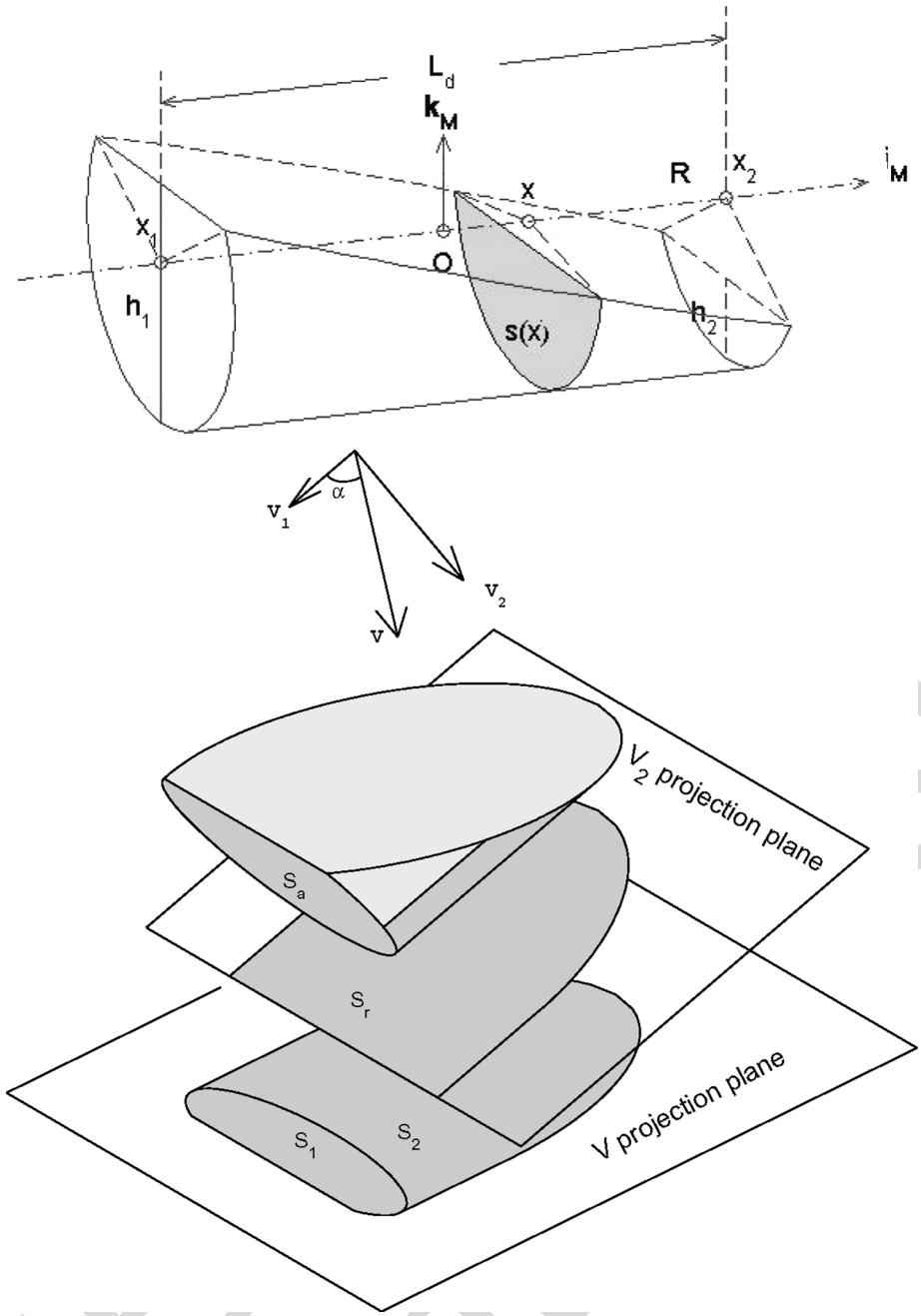

Fig. 14. Calculation of immersed area.

The sediment resistance torque includes the hydrodynamic and shearing resistance torques

$$\mathbf{M}^s = \mathbf{r} \times (\mathbf{F}_r^s + \mathbf{F}_h^s) = -[N(p,v)SA]\,\mathbf{r} \times \boldsymbol{\tau} + \mathbf{r} \times \mathbf{F}_h^s. \quad (25)$$

Here, p is the nondimensional penetration depth scaled by the diameter of the cylinder $(2R)$. The sediment density in (23) and shear strength (S) in (24) and (25) are measured.

The bearing factor increases with p and decreases with the decreasing speed

$$N(p,v) = [\mu_1 p^{\mu_2}] \left[1 + \lambda \log\left(\frac{v}{v_{\text{cri}}}\right)\right] \quad (26)$$

where λ is the v-effect parameter, (μ_1, μ_2) are the p-effect parameters [16], and v_{cri} is the critical speed. The bearing factor N is amplified $[1 + \lambda \log(v/v_{\text{cri}}) > 1]$ for $v > v_{\text{cri}}$, independent of v for $v = v_{\text{cri}}$, and is reduced $[1 + \lambda \log(v/v_{\text{cri}}) < 1]$ for $v < v_{\text{cri}}$. During the penetration, v decreases since the buoyancy, hydrodynamic, and shear resistance forces oppose the penetration. Decrease of v reduces bearing factor N. The two p-effect parameters are given by [16]

$$\mu_1 = 9.3 \quad \mu_2 = 0.7.$$

Note that the nondimensional (26) and the two p-effect parameters are derived from a small probe under axial impact condi-

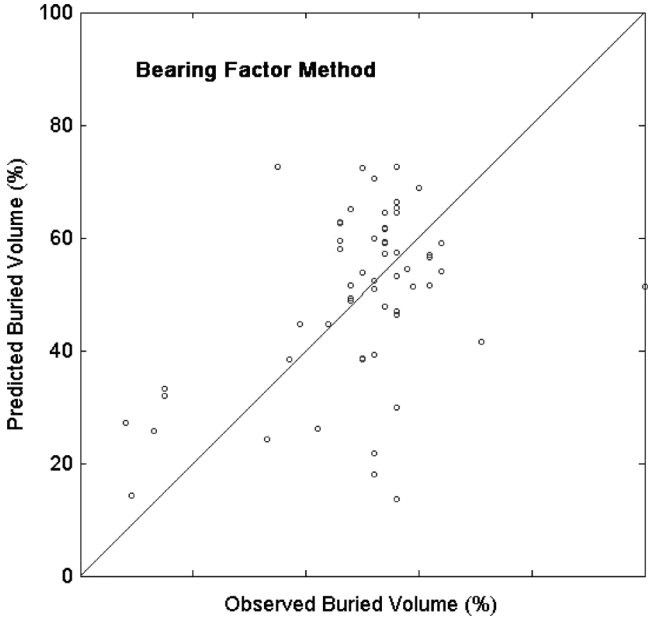

Fig. 15. Scatter diagrams of buried volume prediction against the Baltic Sea Experiment data. Here, IMPACT35 uses the bearing factor method for sediment resistance.

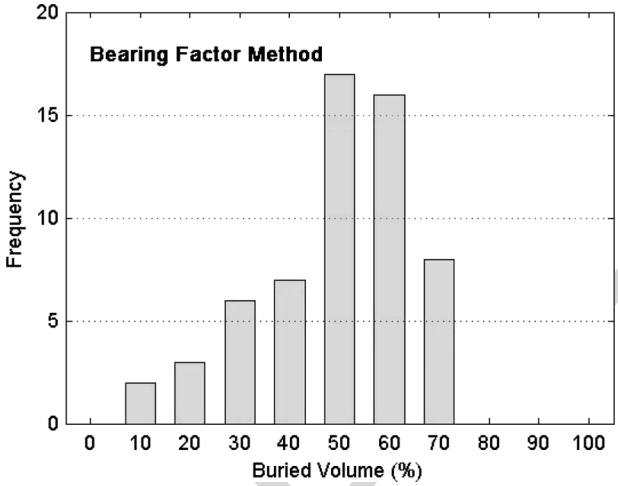

Fig. 16. Histogram of buried volume (in percent) prediction using IMPACT35 with the delta method.

tion. Validity of the bearing factor method to mine impact burial needs thorough evaluation.

Since N cannot be negative, when v decreases to a critical

$$v = v_{\text{cri}} e^{-\frac{1}{\lambda}} \tag{27}$$

the bearing factor $N(p, v)$ and in turn the shearing resistance force become zero. The mine ceases the penetration in sediment. Note that λ and v_{cri} are the two tuning parameters of the numerical model. In this paper, we use

$$\lambda = 0.2 \quad v_{\text{cri}} = 0.0015 \text{ m s}^{-1}. \tag{28}$$

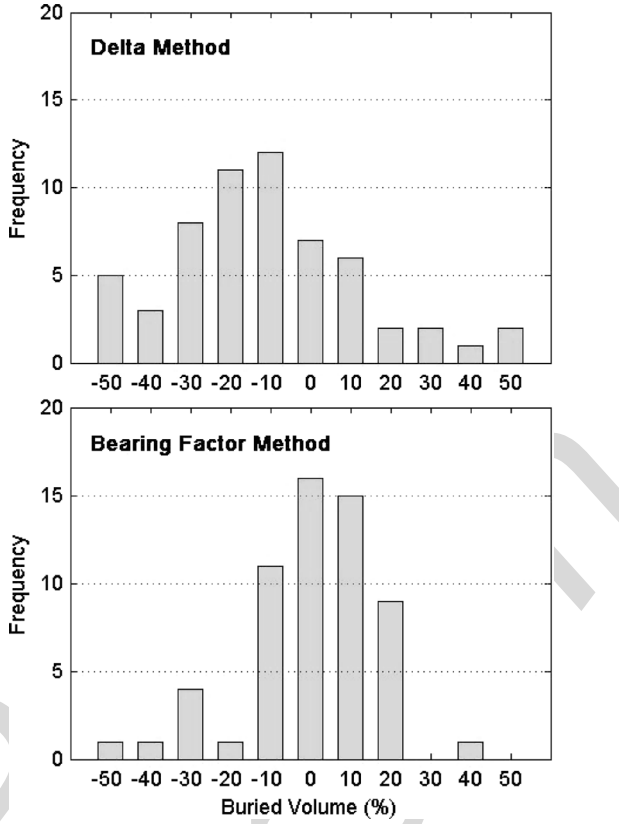

Fig. 17. Histograms of the buried volume prediction error of IMPACT35 using (a) the delta method, and (b) the bearing factor method.

B. Rupture Area

Usually, after passing through the water column, the cylinder's velocity reduces. The rupture area can be represented approximately by the contact surface area. Let (A_f, A_t) be the sediment-contacting areas on the circular bottom (fan shape) and side (curved trapezoid). The rupture area A is the summation of the projections of (A_f, A_t) on the plane perpendicular to the mine's velocity $\mathbf{V}$

$$A = A_1 + A_2 \quad A_1 = A_f \cos\alpha \quad A_2 = A_t \sin\alpha \tag{29}$$

where α is the angle between $\mathbf{V}$ and the mine's axis. Let R be the radius of the cylinder, h be the depth of A_f, and (h_1, h_2) be the depths of the trapezoid A_t immersed in the sediment (Fig. 14). Let the length of the trapezoid be L_t. A_f is computed simply by

$$A_f = \frac{\theta}{2} R^2 - (R-h)\sqrt{R^2-(R-h)^2}, \qquad \theta = \cos^{-1}\left(\frac{R-h}{R}\right). \tag{30}$$

A_t is computed by

$$A_t = \begin{cases} 2L_t R, & \text{for } h_1 > h_2 \geq R \\ \frac{L_t}{(h_1 - h_2)}\left[R^2(\theta_1 - \theta_2)\right. & \\ \quad \left. -(R-h_1)b_1 + (R-h_2)b_2\right], & \text{for } h_2 < h_1 \leq R \\ 2L_{t1}R + \frac{L_{t2}}{(R-h_2)} & \\ \quad \times \left[R^2\left(\frac{\pi}{2} - \theta_2\right) + (R-h_2)b_2\right], & \text{for } h_1 > R > h_2 \end{cases} \tag{31}$$

where (L_{t1}, L_{t2}) are the lengths of subcylinders with $(h > R, h < R)$ and b_1 and b_2 are computed by

$$b_1 = \sqrt{R^2 - (R-h_1)^2} \quad b_2 = \sqrt{R^2 - (R-h_2)^2}. \tag{32}$$

VI. Model Improvement Using the Bearing Factor Method

Model improvement is evaluated using the Baltic Sea experiment data. Similar to the process described in Section V, the modeled (with the bearing factor method) and observed burial volumes (in percent) were compared (Fig. 15). As evident, the sediment resistance using the bearing factor method improves the prediction capability of IMPACT35. The bias (mean predicted minus observed values) and rmse of the burial volume reduce to 0.1% and 15.8%. The correlation coefficient between observed and predicted burial volumes increases to 0.435 (using the bearing factor method) from 0.374 (using the delta method).

The histogram of the predicted burial volume (in percent) using the bearing factor method (Fig. 16) is closer to that of the Baltic Sea experiment [Fig. 13(a)] than the histogram of the predicted burial volume (in percent) using the delta method Fig. 13(b). In the experiment, the histogram has a peak at burial volume of 50% with a frequency of 26. In the prediction, the histogram has a peak at 30% with a frequency of 11 using the delta method Fig. 13(b). However, the histogram has a peak at 50% with a frequency of 17% (Fig. 16).

The histogram of the model error is more symmetric around the zero error using the bearing factor method than using the delta method. For example, the histogram has a peak at zero error with frequency of 16 using the bearing factor method [Fig. 17(b)], and a peak at -10% error with the frequency of 12 using the delta method [Fig. 17(a)]. The burial volume prediction is unbiased using the bearing factor method, and negatively biased using the delta method.

VII. Summary

The following points summarize this paper.

1) The 3-D mine impact burial prediction model (IMPACT35) was recently developed to predict the translation and orientation of falling cylindrical mine through air, water, and sediment. It contains the following three components: triple coordinate transform, cylinder decomposition, and hydrodynamics of falling rigid object in a single medium (air, water, or sediment) and in multiple media (air–water and water–sediment interfaces).
2) Data collected from two mine impact burial experiments were used to verify the existing IMPACT35. The predicted mine track and orientation in the water column agree quite well with the NSWC-Caderock data. The rmse of mine's position and orientation is much smaller using IMPACT35 than using IMPACT28. However, the predicted mine burial volume in the sediment was not as good as the mine trajectory in the water column.
3) Calculation of the sediment resistant force and torque is updated from the delta method (old) to the bearing factor method (new). With the bearing factor method, the prediction capability of IMPACT35 has been greatly improved. The prediction error satisfies near-Gaussian distribution. The bias of the burial volume (in percent) prediction reduces from 11% using the delta method (old) to 0.1% using the bearing factor method. Correspondingly, the rmse reduces from 26.8% to 15.8%.
4) IMPACT35 developed in this paper is only for cylindrical mines only. It is necessary to extend the modeling effort to more realistic mine shapes such as Rockan and Manta for operational use.

Acknowledgment

The authors would like to thank Dr. P. Valent and Dr. A. Abelev at the NRL for providing the NSWC-Carderock experiment data, Dr. T. Weaver at the FWG for providing the Baltic Sea experiment data, and the two anonymous reviewers and the editor Dr. M. D. Richardson for comments that improved the manuscript greatly.

References

[1] J. M. Boorda, *Mine Countermeasures—An Integral Part of Our Strategy and Our Forces*. Washington, DC: Federation of American Scientists, 1999 [Online]. Available: http://www.fas.org/man/dod-101/sys/ship/weaps/docs/cnopaper.htm

[2] ***[Page range to come!]*** S. A. Jenkins, D. L. Inman, M. D. Richardson, T. F. Wever, and J. Wasyl, "Scour and burial mechanisms of objects in the nearshore," *IEEE J. Ocean. Eng.*, vol. 32, no. 1, pp. XXX–XXX, Jan. 2007.

[3] ***[Page range to come!]*** P. C. Chu, "Mine impact burial prediction from one to three dimensions," *IEEE J. Ocean. Eng.*, vol. 32, no. 1, pp. XXX–XXX, Jan. 2007.

[4] ***[Page range to come!]*** S. E. Rennie, A. Brandt, and N. Plant, "A probabilistic expert system approach for sea mine burial prediction," *IEEE J. Ocean. Eng.*, vol. 32, no. 1, pp. XXX–XXX, Jan. 2007.

[5] S. Haeger, "Operational ocean modeling support for mine warfare in operation Iraqi freedom," in *Proc. 6th Int. Symp. Technol. Mine Problem*, Monterey, CA, May 10–13, 2004, DVD-ROM.

[6] ***[AU: Please provide page range]*** P. Fleischer, "Mine burial prediction NAVOCEANO perspective," in *Proc. 5th Annu.ONR Workshop Mine Burial Prediction*, Kona, HI, Jan. 31–Feb. 2 2005.

[7] ***[Page range to come!]*** P. A. Elmore, M. D. Richardson, and R. H. Wilkens, "Exercising the Monte Carlo mine burial prediction system for impact and scour burial for operational Navy use," *IEEE J. Ocean. Eng.*, vol. 32, no. 1, pp. XXX–XXX, Jan. 2007.

[8] ***[AU: Please provide department]*** T. B. Smith, "Validation of the mine impact burial model using experimental data," M.S. thesis, Naval Postgrad. School, Monterey, CA, 2000.

[9] P. C. Chu, C. W. Fan, A. D. Evans, and A. F. Gilles, "Triple coordinate transforms for prediction of falling cylinder through the water column," *J. Appl. Mech.*, vol. 71, pp. 292–298, 2004.

[10] P. C. Chu, A. F. Gilles, C. W. Fan, J. Lan, and P. Fleischer, "Hydrodynamics of falling cylinder in water column," *Adv. Fluid Mech.*, vol. 4, pp. 163–181, 2002.

[11] P. C. Chu, A. F. Gilles, C. W. Fan, and P. Fleischer, "Hydrodynamics of falling mine in water column," in *Proc. 4th Int. Symp. Technol. Mine Problem*, 2000, CD-ROM.

[12] P. C. Chu and C. W. Fan, "Pseudo-cylinder parameterization for mine impact burial prediction," *J. Fluids Eng.*, vol. 127, pp. 1515–1520, 2005.

[13] ——, "Prediction of falling cylinder through air-water-sediment columns," *J. Appl. Mech.*, vol. 73, pp. 300–314, 2006.

[14] P. C. Chu, A. F. Gilles, and C. W. Fan, "Experiment of falling cylinder through the water column," *Exp. Thermal Fluid Sci.*, vol. 29, pp. 555–568, 2005.

[15] ***[AU: Please provide department]***A. Evans, "Hydrodynamics of mine impact burial," M.S. thesis, Monterey, CA, 2002.

[16] ***[Page range to come!]***C. P. Aubeny and H. Shi, "Effect of rate-dependent soil strength on cylinders penetrating into soft clay," *IEEE J. Ocean. Eng.*, vol. 32, no. 1, pp. XXX–XXX, Jan. 2007.

[17] P. C. Chu, C. W. Fan, and A. D. Evans, "Three-dimensional rigid body impact burial model (IMPACT35)," *Adv. Fluid Mech.*, vol. 6, pp. 43–52, 2004.

[18] P. C. Chu, A. Evans, T. Gilles, T. Smith, and V. Taber, "Development of Navy's 3D mine impact burial prediction model (IMPACT35)," in *Proc. 6th Int. Symp. Technol. Mine Problem*, Monterey, CA, 2004, DVD-ROM.

[19] ***[AU: This is the same reference as [13]. Please advise.]***P. C. Chu and C. W. Fan, "Prediction of falling cylinder through air-water-sediment columns," *J. Appl. Mech.*, vol. 73, pp. 300–314, 2006.

[20] ***[Page range to come!]***A. V. Abelev, P. J. Valent, and K. T. Holland, R. H. Wilkens and M. D. Richardson, Eds., "Behavior of a large cylinder in free fall through water," *IEEE J. Ocean. Eng.*, vol. 32, no. 1, pp. XXX–XXX, Jan. 2007.

[21] K. T. Holland, A. W. Green, A. Abelev, and P. J. Valent, "Parameterization of the in-water motions of falling cylinders using high-speed video," *Exp. Fluids*, vol. 37, pp. 690–770, 2004, doi: 10.1007/800348-004-0859-2.

[22] ***[AU: Please provide page range]***P. A. Elmore, R. Wilkens, T. Weaver, and M. D. Richardson, "IMPACT 28 and 35 simulations of 2003 Baltic Sea cruise: Model results and comparison with data," in *Proc. 5th Annu. ONR Workshop Mine Burial Prediction*, Kona, HI, Jan. 31– Feb. 2 2005.

[23] A. Palmer, "Speed effect in cutting and ploughing," *Geotechnique*, vol. 49, no. 3, pp. 285–294, 1997.

[24] B. C. Simonsen and N. E. O. Hansen, "Protection of marine structures by artificial islands," in *Ship Collision Analysis*, Gluver and Olsen, Eds. Rotterdam, The Netherlands: Balkema, 1998, pp. 201–215, ISBN: 9054109629.

[25] ***[AU: Please provide page range]***T. Wever, "Surprising mine burial observations at MVCO," in *Proc. 5th Annu. ONR Workshop Mine Burial Prediction*, Kona, HI, Jan. 31– Feb. 2 2005.

Peter C. Chu received the Ph.D. degree in geophysical fluid dynamics from the University of Chicago, Chicago, IL, in 1985.

He is a Professor of Oceanography and Head of the Naval Ocean Analysis and Prediction (NOAP) Laboratory, the Naval Postgraduate School, Monterey, CA. His research interests include ocean analysis and prediction, coastal modeling, littoral zone oceanography for mine warfare, mine impact burial prediction, mine acoustic detection, and satellite data assimilation for undersea warfare.

Chenwu Fan received the M.S. degree in mechanic engineering from China Textile University ***[AU: Please provide location of the university]*** in 1982.

He is an Oceanographer at the Naval Postgraduate School, Monterey, CA. His research interests include numerical simulation, ocean analysis and prediction, coastal modeling, littoral zone oceanography for mine warfare, and mine impact burial prediction.